© 2019. Published by The Company of Biologists Ltd | Development (2019) 146, dev174508. doi:10.1242/dev.174508

RESEARCH ARTICLE

A V0-ATPase-dependent apical trafficking pathway maintains the polarity of the intestinal absorptive membrane

Aurélien Bidaud-Meynard, Ophélie Nicolle, Markus Heck, Yann Le Cunff and Grégoire Michaux*

ABSTRACT

Intestine function relies on the strong polarity of intestinal epithelial cells and the array of microvilli forming a brush border at their luminal pole. Combining a genetic RNA interference (RNAi) screen with *in vivo* super-resolution imaging in the *Caenorhabditis elegans* intestine, we found that the V0 sector of the vacuolar ATPase (V0-ATPase) controls a late apical trafficking step, involving Ras-related protein 11 (RAB-11)$^{+}$ endosomes and the *N*-ethylmaleimide-sensitive factor-attachment protein receptor (SNARE) synaptosome-associated protein 29 (SNAP-29), and is necessary to maintain the polarized localization of both apical polarity modules and brush border proteins. We show that the V0-ATPase pathway also genetically interacts with glycosphingolipids and clathrin in enterocyte polarity maintenance. Finally, we demonstrate that silencing of the V0-ATPase fully recapitulates the severe structural, polarity and trafficking defects observed in enterocytes from individuals with microvillus inclusion disease (MVID) and use this new *in vivo* MVID model to follow the dynamics of microvillus inclusions. Thus, we describe a new function for V0-ATPase in apical trafficking and epithelial polarity maintenance and the promising use of the *C. elegans* intestine as an *in vivo* model to better understand the molecular mechanisms of rare genetic enteropathies.

KEY WORDS: *C. elegans*, Epithelial cells, Intestine, Microvillus inclusion disease, Polarity, Trafficking

INTRODUCTION

Almost all nutrients in the diet are absorbed into blood across the epithelial layer that forms the small and large intestinal mucosa (Kiela and Ghishan, 2016). Therefore, proper establishment and maintenance of both the strong polarity of enterocytes and the array of microvilli forming an absorptive brush border at their apical plasma membrane (PM) are essential to ensure proper intestinal function. In most species, including *Caenorhabditis elegans*, epithelial cell polarity is achieved by actin and microtubule cytoskeleton reorganization, trafficking and signaling-mediated polarized targeting of the cell division cycle 42 (CDC-42)/partitioning defective 3 (PAR-3)/PAR-6/protein kinase C (PKC)-3 (CDC-42/PAR) and Crumbs/PALS1/Patj (CRB) modules at the apical pole and the Dlg/Scribble/Lgl (SCRIB) module at the basolateral pole, as well as domain-specific lipid distribution (Rodriguez-Boulan and Macara, 2014). Of particular importance in polarity maintenance is CDC-42, because it controls the apical localization of PAR module components in the *C. elegans* intestine (Shafaq-Zadah et al., 2012) and Madin–Darby Canine Kidney (MDCK) cysts (Martin-Belmonte et al., 2007). The establishment of the brush border is thought to be dependent on actin cytoskeleton-regulating factors, which create the force necessary for the onset and maintenance of the microvilli (Heintzelman and Mooseker, 1990a, b; Crawley et al., 2014; Saegusa et al., 2014).

Polarity establishment and brush border formation are early events in intestine development, and both rely on related cytoskeletal and trafficking pathways. In *C. elegans*, clathrin and the sigma subunit of the AP-1 clathrin adaptor complex (*aps-1*, Wormbase.org) (Shafaq-Zadah et al., 2012; Zhang et al., 2012), glycosphingolipids (GSLs) (Zhang et al., 2011), the kinase Lats/WTS-1 (Kang et al., 2009) and PAR-5 (Winter et al., 2012) have major roles in the sorting of polarity modules and luminogenesis. In mammalian intestine cellular models, the trafficking proteins annexin 2, syntaxin-3 (STX3), Rab8a and Rab11a, the actin-binding protein Drebrin E, as well as myosins V and VI, have been found to be involved in the polarized localization of PM transporters and brush border integrity (Hegan et al., 2012; Vogel et al., 2015; Vacca et al., 2014; Hein et al., 2011). Moreover, myosin Vb (MYO5B) has also been implicated in the apical confinement of the PAR polarity module (Michaux et al., 2016).

In particular, these studies have highlighted the central role of Ras-related protein 11 (RAB-11)-dependent apical trafficking in polarity maintenance and lumen integrity. Indeed, studies in MDCK cells demonstrated the crucial function of RAB 11^{+} endosomes in apical PM and lumen generation via their mediation of PAR-3 targeting and CDC-42 activation through the exocyst complex (Colombié et al., 2017; Bryant et al., 2010) as well as the adverse effect of dominant-negative *Rab11* (*Rab11*^{DN}) expression on the apical localization of phospho-ezrin and E-Cadherin (cadherin 1) (Desclozeaux et al., 2008). Furthermore, expression of *Rab11*^{DN} or depletion of the Rab11^{+} endosome-associated motor MYO5B decreased both ezrin phosphorylation at the apical PM and microvilli size in intestinal cell models (Dhekne et al., 2014). These polarity and structural consequences were further confirmed in a *Rab11a* intestinal-specific knockout (KO) mouse model (Sobajima et al., 2015). Finally, defective RAB-11-dependent trafficking has been associated with congenital enteropathies, which are characterized by polarity and brush border structural defects (Vogel et al., 2017a). However, little is known about the relationship between polarity modules, brush border and apical trafficking components and their sequential involvement in establishing and maintaining an absorptive intestinal apical PM, especially *in vivo*.

The *C. elegans* intestine comprises 20 polarized enterocytes, similar to those in the mammalian intestine, and the nematode embryonic and larval stages have been widely used to understand polarity and lumen establishment and maintenance, respectively (McGhee, 2007). By performing an RNA interference (RNAi) screen to target a library of trafficking and cytoskeleton factors in

Univ Rennes, CNRS, IGDR (Institut de Génétique et Développement de Rennes) - UMR 6290, F-35000 Rennes, France.

*Author for correspondence (gmichaux@univ-rennes1.fr)

A.B.-M., 0000-0003-0103-3827; G.M., 0000-0003-1222-5461

Received 3 December 2018; Accepted 7 May 2019

Development (2019) 146, dev174508. doi:10.1242/dev.174508

C. elegans larvae, we found that the silencing of the V0 sector of the vacuolar ATPase (V-ATPase) induced a cytoplasmic and basolateral mislocalization of both the PAR polarity module and brush border components. V-ATPase is a large heteromultimeric complex [20 subunits in *C. elegans*: *vha-1* to *vha-18*, defective SPErmatogenesis (*spe*-5) and UNCoordinated (*unc-32*)], organized into two main sectors: a V1 sector (V1-ATPase), which is responsible for the ATP hydrolysis that provides energy to the V0 sector (V0-ATPase), which transports protons (Lee et al., 2010). As a whole, the V-ATPase complex is responsible for the acidification of intracellular compartments, such as endosomes or lysosomes, and has a major role in PM protein trafficking (Maxson and Grinstein, 2014). Additionally, V0-ATPase has also been implicated in the fusion of vesicles to the yeast vacuole (Baars et al., 2007) as well as that of synaptic vesicles in *Drosophila* and humans (Hiesinger et al., 2005; Di Giovanni et al., 2010), in an acidification-independent manner. In *C. elegans*, the V0-ATPase subunits *vha-5*, *vha-6* and *vha-19* are required for exosome-containing vesicle apical exocytosis in the epidermis (Liégeois et al., 2006), intestinal lumen pH regulation (Allman et al., 2009) and RME-2 receptor trafficking in oocytes (Knight et al., 2012). However, no role in polarity maintenance has so far been assigned to this complex.

We also show that interfering with the V0-ATPase-mediated polarity maintenance pathway in *C. elegans* fully recapitulates the polarity, trafficking and structural phenotypes observed in patients with microvillus inclusion disease [MVID; Online Mendelian Inheritance in Man (OMIM): 251850]. MVID is caused by mutations in the genes encoding the apical trafficking factors *MYO5B* (Müller et al., 2008), *STX3* (Wiegerinck et al., 2014) or syntaxin binding protein 2 (*MUNC18-2*/*STXBP2*) (Vogel et al., 2017b), and is characterized by microvillus atrophy, the formation of rare microvillus inclusions, and loss of subapical RAB-11^{+} endosomes (Schneeberger et al., 2018). Hence, we describe here a new essential function for V0-ATPase in the control of apical trafficking, polarity maintenance and brush border integrity.

RESULTS

V0-ATPase silencing affects the polarity of brush border and polarity components in the *C. elegans* intestine

To identify new common regulators of polarity and brush border maintenance *in vivo*, we performed a two-step RNAi screen targeting 408 genes essential for survival, conserved in humans and implicated in membrane trafficking and cytoskeleton regulation (Table S5). First, we examined the effect of their silencing on the localization of the polarity module component CDC-42 at the apical PM of enterocytes of *C. elegans* larvae. We then performed a secondary screen to evaluate the ability of the hits decreasing CDC-42 apical localization to also disturb the polarity of the brush border-specific actin crosslinker Ezrin/Radixin/Moesin (ERM-1) (Table S1 and Fig. S1A,B). This systematic RNAi screen first confirmed the involvement of clathrin (*chc-1*), AP-1 (*aps-1*; the σ subunit of AP-1) and GSL biosynthesis enzymes [i.e. Serine Palmitoyl Transferase family (*sptl-1*), Fatty Acid SyNthase (*fasn-1*) and Polarity and Osmotic sensitivity Defect (*pod-2*)] (Zhang et al., 2012, 2011; Shafaq-Zadah et al., 2012) in the maintenance of intestinal polarity and identified several genes belonging to the biosynthetic and endocytic pathways, as well as ten subunits of the V-ATPase complex, which regulates endosomal acidification in intracellular trafficking (Table S1). The results of this screen using overexpressed markers were then confirmed by silencing several subunits of the V-ATPase complex and studying the endogenous localization of genome-edited mNeonGreen (mNG)-tagged ERM-1 and Green Fluorescent Protein (GFP)-tagged polarity module components PAR-6 and PKC-3. Consistently, knockdown of subunits from both the V0 and V1 sectors of V-ATPase complex decreased by 15-40% the apical/cytoplasmic ratio of the PAR module proteins and of ERM-1, whereas direct alkalinization of the *C. elegans* intestine using ammonium chloride or chloroquine did not (Fig. 1A-F and Fig. S1C,D). This indicates that the whole V-ATPase complex is involved in the apical confinement of brush border and polarity module components, probably through its canonical acidification-dependent trafficking mechanism. Intriguingly, knockdown of the V0-ATPase subunits *vha-1*, *vha-4* and *vha-19* also induced a basolateral localization of ERM-1, whereas no basolateral mislocalization was observed upon silencing of the V1-ATPase subunits *vha-8* (hereafter V1/*vha-8*) and *vha-15* (Fig. 1A,G). Importantly, *vha-8* depletion has been shown to inhibit V-ATPase-dependent acidification (Ji et al., 2006). This phenotype was obvious only after 72 h RNAi (Fig. S1E), which corresponded to the time needed to significantly downregulate the expression of the *vha* subunits (Fig. S1F). Furthermore, endogenous PAR-6 and PKC-3 were also specifically observed at the basolateral PM in ∼20% of the worms upon V0-ATPase subunit silencing (Fig. 1B,C). These observations suggest a specific V0-ATPase function to prevent the localization of essential structural and polarity proteins at the basolateral PM, whereas all V-ATPase subunits are required to prevent their cytoplasmic mislocalization. To evaluate whether V0-ATPase silencing induces a global polarity inversion of enterocytes, we studied the effect of the silencing of the V0-ATPase subunit *vha-1* (hereafter V0/*vha-1*), which destabilized the whole V0-ATPase sector (Fig. S1G,H) on the polarized localization of the apical peptide transporter PEPTide transporter family (PEPT-1; OPT-2) and the P-glycoprotein, P-GlycoProtein related (PGP-1) as well as the basolateral pyruvate transporter SoLute Carrier Family (SLCF-1). Notably, silencing of V0/*vha-1* did not have a significant effect on the cortical confinement of those highly polarized proteins and none of them accumulated at the contralateral PM (Fig. 1H-K and Fig. S1I,J), supporting the hypothesis that enterocyte polarity is only partially compromised upon V0/*vha-1* silencing. Overall, these data indicate that V0-ATPase specifically controls the polarized localization of both brush border (ERM-1) and polarity module components (PAR-6 and PKC-3) in enterocytes.

V0-ATPase silencing specifically affects the apical recycling pathway

The V-ATPase complex controls the acidification of various endosomes along the biosynthetic and endocytic-recycling routes (Forgac, 2007). Using transmission electron microscopy (TEM), we observed the presence of abnormal large organelles (0.1-0.3 µm in diameter with variable electron density and heterogeneous content) with features of endosomes and lysosomes upon inhibition of both the V0/*vha-1* and V1/*vha-8* subunits (Fig. 2A,B). These 'mixed' organelles have been already described in the *C. elegans* epidermis and in mammalian cells upon V0-/V1-ATPase silencing or chemical inhibition of the V-ATPase complex function, and have been proposed to affect protein sorting along the secretory and lysosomal pathways (Sobota et al., 2009; Liégeois et al., 2006), probably because of the failure of endosome acidification. The presence of mixed organelles was confirmed by the accumulation of several endosomal markers in large cytoplasmic structures, such as lysosome-associated membrane protein (LMP-1; lysosomes), RAB-7 (late endosomes) and RAB-10 (basolateral recycling endosomes) (Fig. 2C and Fig. S2A), upon either V0/*vha-1* or V1/*vha-8* silencing.

Development (2019) 146, dev174508. doi:10.1242/dev.174508

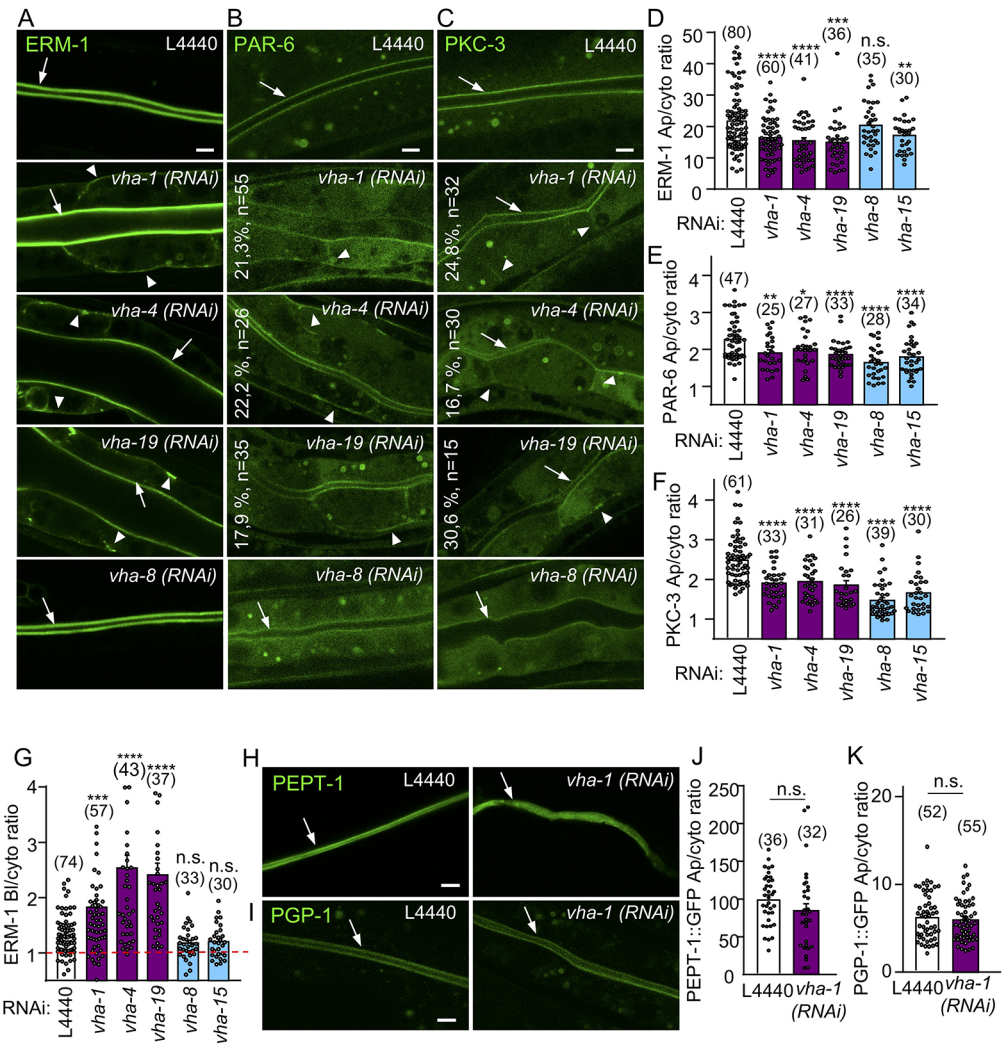

Fig. 1. V0-ATPase controls the apical localization of polarity and brush border components. (A-C) Larvae expressing endogenous ERM-1::mNG, PAR-6::GFP and GFP::PKC-3 were imaged after 72 h silencing of V0/*vha-1*(*RNAi*) or V1/*vha-8*(*RNAi*) subunits. The percentage of worms displaying basolateral PAR polarity markers and the number of worms analyzed are indicated on each panel. (D-F) Quantification of the apical/cytoplasmic ratio of ERM-1::mNG (D), PAR-6::GFP (E) and GFP::PKC-3 (F) upon 72 h silencing of V0-ATPase (*vha-1*, *vha-4* and *vha-19*) or V1-ATPase (*vha-8* and *vha-15*) subunits (*n*=3-5 independent experiments). (G) V0-ATPase subunit (*vha-1*, *vha-4* and *vha-19*) knockdown specifically induced the basolateral relocalization of ERM-1. Histogram shows the basolateral/cytoplasmic ratio of ERM-1::mNG (*n*=3-5 independent experiments). Dotted red line indicates a ratio of 1, which means no basolateral localization. (H-K) V0-ATPase silencing did not affect the polarity of the apical transmembrane proteins PEPT-1 and PGP-1. Strains expressing exogenously (PEPT-1)- or endogenously (PGP-1)-tagged markers were silenced for V0/*vha-1* for 72 h and then imaged. Histograms in (J-K) represent the quantification of the apical/cytoplasmic ratio (*n*=3 independent experiments). Arrows and arrowheads indicate the intestinal apical PM and the basolateral mislocalization of markers upon V0/*vha-1*(*RNAi*), respectively. In all micrographs, worms are at the L4/young adult developmental stage. Note that the lumen sometimes displayed a dilatation upon knockdown of all V-ATPase subunits and in all strains. Histograms show mean±s.e.m., dots represent individual worms and the total number of worms is indicated in brackets. n.s., nonsignificant, **P*<0.05, ***P*<0.01, ****P*<0.001, *****P*<0.0001. Scale bars: 5 µm.

Strikingly, V0/*vha-1* but not V1/*vha-8* silencing led to the specific accumulation of electron-lucent vesicular structures in the cytoplasm (Fig. 2D), which were reminiscent of an apical trafficking defect. The number of RAB-5^{+} endosomes was slightly decreased upon either V0/*vha-1* or V1/*vha-8* silencing, whereas *rab-5*(*RNAi*) did not affect ERM-1 apical polarity (Fig. 2E,F and Fig. S2B). However, RAB-11^{+} endosomes all but disappeared from the apical PM and accumulated in the cytoplasm upon V0/*vha-1*, *vha-4* and *vha-19* but not V1/*vha-8* knockdown (Fig. 2G,H and Fig. S2C). Given that *rab-11* knockdown also induced a basolateral mislocalization of ERM-1 (Fig. 2I,J and Fig. S2D,E), similar to V0/*vha-1*(*RNAi*) (Fig. 1A,G), we hypothesized that V0-ATPase controls the localization of polarity determinants and structural proteins by regulating a late trafficking step that also requires RAB-11^{+} endosomes.

SNAP-29 is involved in V0-ATPase-mediated polarity maintenance

To identify other molecular components of the V0-ATPase-mediated intestinal polarity maintenance pathway beyond the interaction with RAB-11, the effects of silencing either V0/*vha-1* or V1/*vha-8* were investigated on several soluble trafficking factors with a highly polarized localization. The PM localizations of CHC-1/clathrin and the syntaxin UNC-64 (the presumptive mammalian STX3 ortholog) were decreased and increased, respectively (Fig. 3A,B), whereas that of the syntaxin SYX-1 (SYN-1) was

Development (2019) 146, dev174508. doi:10.1242/dev.174508

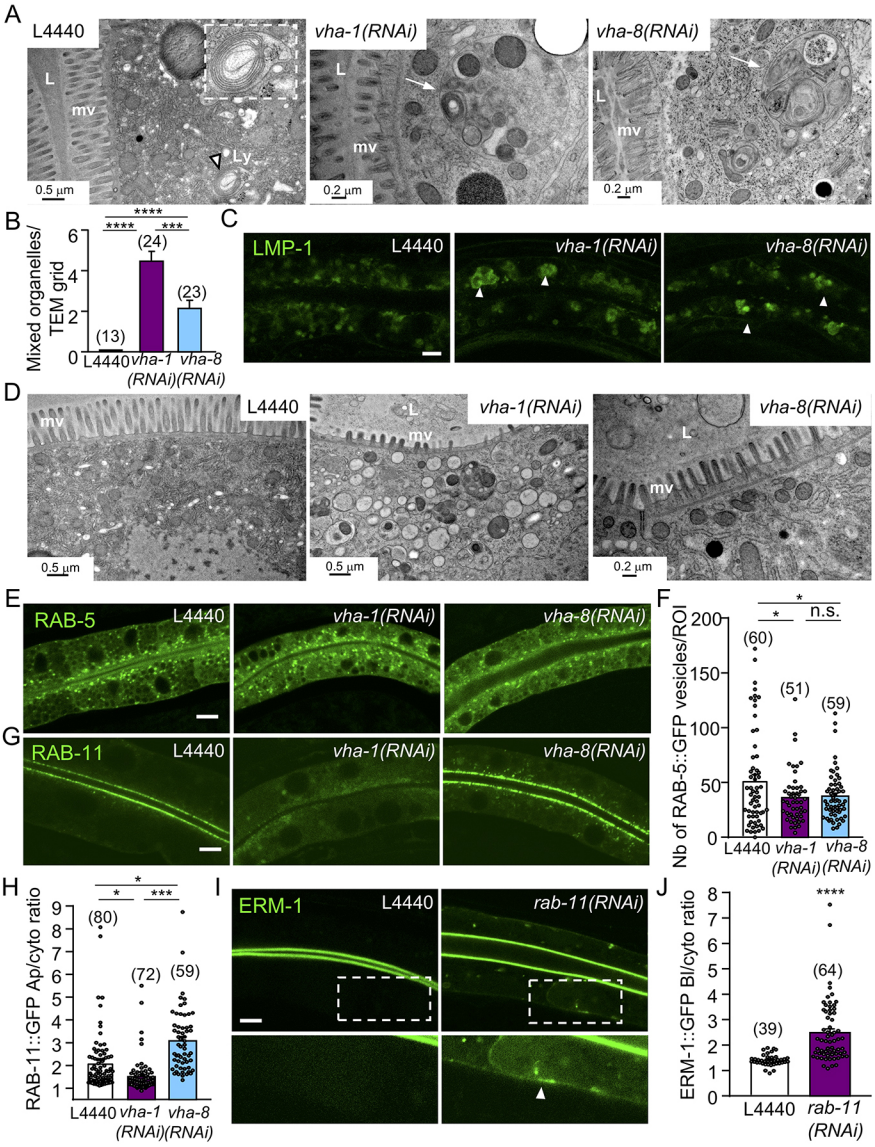

Fig. 2. V0-ATPase affects apical trafficking via RAB-11 apical recycling endosomes. (A-C) V-ATPase complex silencing affects the morphology of lysosomes. (A) Ultrastructural characterization of transversely sectioned control (L4440), V0/*vha-1*- or V1/*vha-8*-depleted worms (72 h RNAi). Whereas lysosomes with normal morphology and size (∼0.5µm) were rarely observed in control worms (left panel, arrowhead and insert), cytoplasmic-enlarged 'mixed organelles' with distinct lysosomal and vesicular regions were observed upon either V0/*vha-1*(*RNAi*) or V1/*vha-8*(*RNAi*) (arrows). (B) Quantification of the number of mixed organelles. Numbers correspond to the total number of TEM grids analyzed (n=1-5 grid/larvae), out of n=7-13 larvae/condition. (C) The accumulation of the lysosomal marker LMP-1::GFP in large cytoplasmic structures (arrowheads) upon both V0/*vha-1* and V1/*vha-8*(*RNAi*). (D) Ultrastructural characterization of transversely sectioned control (L4440), V0/*vha-1*- and V1/*vha-8*-depleted worms (72 h). The middle panel shows the specific and massive accumulation of cytoplasmic electron-lucent vesicles upon V0/*vha-1*(*RNAi*). (E-H) V0- or V1-ATPase silencing marginally decreased the number of RAB-5^{+} vesicles but V0-ATPase knockdown specifically disrupted RAB-11^{+} apical recycling endosomes. Confocal imaging of the endosomal markers of apical early/sorting (RAB-5, E) and apical recycling (RAB-11, G) endosomes in control, V0/*vha-1*(*RNAi*) and V1/*vha-8*(*RNAi*) conditions (72 h). (F,H) Quantification of the number of RAB-5^{+} vesicles (F) and RAB-11 apical/cytoplasmic ratio (H, Mann–Whitney *U*-test) (n=3). (I-J) *rab-11*(*RNAi*) phenocopied V0-ATPase silencing on ERM-1::GFP polarity. ERM-1::GFP-expressing worms were silenced for *rab-11* for 72 h and then imaged. Arrowheads show the basolateral accumulation of ERM-1. (J) ERM-1 basolateral/cytoplasmic ratio quantification (n=3). In all micrographs, worms are at the L4/young adult developmental stage. Histograms are mean±s.e.m.; on each panel, dots represent individual worms and the total number of worms is indicated in brackets (except B). L, lumen; mv, microvilli; Ly, lysosome. n.s., nonsignificant, *P<0.05, ***P<0.001, ****P<0.0001. Scale bars: 0.2 µm or 0.5 µm in A,D; 5 µm in C,E,G,I.

only slightly decreased (Fig. S3A,B) upon silencing of any V-ATPase complex subunit, suggesting a trafficking defect, but no sector specificity. Strikingly, V0/*vha-1*(*RNAi*) specifically decreased the apical localization of the soluble *N*-ethylmaleimide-sensitive factor-attachment protein receptor (SNARE) component synaptosome-associated protein 29 (SNAP-29), whereas V1/*vha-8*(*RNAi*) did not (Fig. 3C). SNAP-29 belongs to the SNAP23/25/29 family of SNARE proteins that interact with syntaxins and SEC/MUNC proteins to promote vesicle fusion (Sudhof and Rothman, 2009). Its silencing affects the morphology of various organelles, including recycling endosomes and, consequently, endocytosis, secretion as well as autophagy pathways in the *C. elegans* intestine (Sato et al., 2011; Guo et al., 2014). Furthermore, *snap-29* was a positive candidate in our polarity screen (Table S1 and Fig. S3C). To confirm that SNAP-29 is involved in polarity maintenance, *snap-29* was silenced by RNAi (Fig. S3D,E) and the PM

Development (2019) 146, dev174508. doi:10.1242/dev.174508

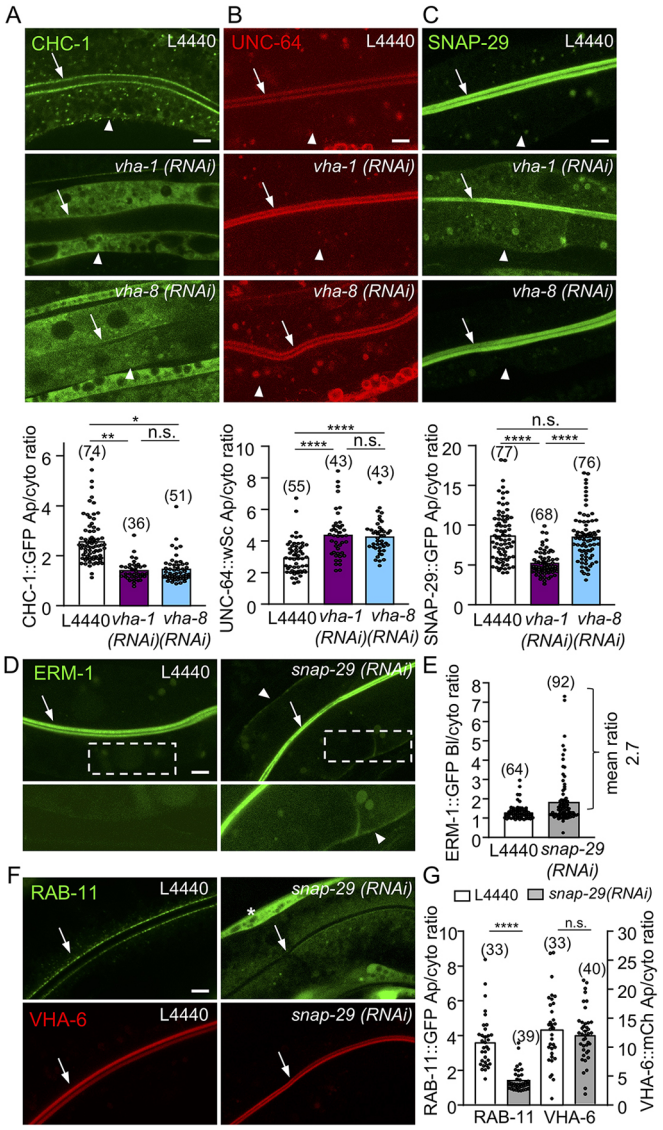

Fig. 3. SNAP-29 acts downstream of V0-ATPase in polarity maintenance. (A-C) V0-ATPase silencing specifically decreased the apical localization of GFP::SNAP-29. Strains expressing the indicated markers were silenced for V0/*vha-1* or V1/*vha-8* ATPase for 72 h and then imaged. Histograms represent the quantification of the apical/cytoplasmic ratio of each marker (*n*=3). (D-E) *snap-29*(*RNAi*) induced a basolateral mislocalization of ERM-1. *snap-29* was knocked down by RNAi in ERM-1::GFP-expressing strains and its localization was recorded after 72 h. (E) The quantification of the basolateral/cytoplasmic ratio of ERM-1::GFP (*n*=5). (F-G) *snap-29*(*RNAi*) also induced a RAB-11^{+} endosomes loss but did not affect VHA-6 apical localization. *snap-29* was depleted by RNAi in a strain co-expressing GFP::RAB-11e and VHA-6::mCh. The asterisk indicates a muscular Myo-3P::GFP co-expressed with VHA-6::mCh. (G) The quantification of GFP::RAB-11e (left panel) and VHA-6::mCh (right panel) apical/cytoplasmic ratio (*n*=2). In all micrographs, worms are at the L4/young adult developmental stage. Arrows and arrowheads indicate the apical PM and the basolateral PM, respectively. Histograms are mean±s.e.m.; on each panel, dots represent individual worms and the total number of worms is indicated in brackets. n.s., nonsignificant, **P*<0.05, ***P*<0.01, *****P*<0.0001. Scale bars: 5 µm.

localization of ERM-1 was assessed. *snap-29* silencing induced a basolateral mislocalization of ERM-1 (basolateral/cytoplasmic ratio >1.5) in 35.0% of the worms, whereas only 19.2% of control (L4440) worms displayed a ratio >1.5 (Fig. 3D,E). Finally, the effect of *snap-29*(*RNAi*) was assayed on a strain co-expressing RAB-11::GFP and the V0-ATPase subunit VHA-6::mCh. Whereas *snap-29* knockdown also induced a dramatic loss of RAB-11 signal, it did not affect the V0-ATPase subunit VHA-6 signal (Fig. 3F,G). Hence, these data suggest that SNAP-29 acts downstream of the V0-ATPase to maintain enterocyte polarity.

High-resolution map of the apical PM reveals that V0-ATPase localizes to microvilli

The V0-ATPase VHA-6 subunit has been localized at the apical PM of intestinal epithelia in *C. elegans* (Zhu et al., 2015) and proposed to traffic to the brush border in Caco-2 cells (Collaco et al., 2013). However, conventional confocal imaging in *C. elegans* only enabled researchers to determine the apical polarity of markers, but not their precise position regarding the apical PM (e.g. microvilli, terminal web or subapical). Thus, the precise localization of the V0-ATPase as well as that of some of the above-mentioned polarity markers was assessed by live super-resolution confocal microscopy. This technique confirmed that ERM-1 specifically accumulated in microvilli, whereas ACT-5, PGP-1 and SNAP-29 were present both along and at the base of microvilli (Fig. 4A-C and Fig. S4A). SNAP-29 localizes on RAB-11^{+} endosomes in *C. elegans* intestine (Kang et al., 2011) and this interaction appears to take place at the microvilli base, close to the presumptive terminal web, a network of actin and intermediate filaments running below and in parallel to the apical PM (the electron-dense and intermediate filaments/IFB-2-positive belt underneath the apical PM has been referred to as the 'endotube' in *C. elegans*) (Bossinger et al., 2004), where most of the PAR component PKC-3 accumulates (Fig. 4A-D). Finally, the V0-ATPase subunit VHA-6 localized to the microvilli, above the RAB-11 apical staining (Fig. 4E). Overall, these results suggest that V0-ATPase localizes at microvilli, from where it controls the apical localization of the brush border and polarity modules by regulating a late trafficking step through RAB-11^{+} endosomes in a SNAP-29-dependent manner.

V0-ATPase interacts with GSLs and clathrin in intestinal polarity maintenance

Interestingly, two trafficking and possibly cooperating pathways have been invoked as major regulators of intestinal polarity maintenance in *C. elegans*: GSLs and clathrin/clathrin adaptor AP-1. In particular, silencing of the AP-1 complex subunit *aps-1*, *chc-1* or of enzymes along the GSL biosynthetic pathway [i.e. LEThal (*let-767*), fatty Acid CoA Synthetase family (*acs-1*), *pod-2* or *sptl-1*] has been shown to induce the contralateral PM localization of polarized proteins and a loss of RAB-11^{+} endosomes (Shafaq-Zadah et al., 2012; Zhang et al., 2012, 2011), similar to V0/*vha-1* silencing. To test the putative genetic interactions between the V0-ATPase, GSL and clathrin/AP-1 pathways, V0/*vha-1*, *aps-1* or *chc-1* were co-depleted by RNAi (Fig. S4B) and V0/*vha-1* was silenced in a *let-767*(*s2176*) loss-of-function mutant balanced with the *sDp3* duplication (Zhang et al., 2012). *chc-1* and *aps-1* strongly and slightly mislocalized ERM-1 to the basolateral PM, respectively, whereas the heterozygous *let-767* mutation had no significant effect on ERM-1 polarized localization (Fig. 5A). Notably, the effect of combined *vha-1* and *let-767* knockdowns, as well as that of combined *vha-1* and *chc-1* knockdowns, was significantly different from the addition of their individual effects, which indicates a synergy between these pathways that was not observed between *vha-1* and *aps-1* (Fig. 5B-D). Thus, we conclude that *vha-1* genetically interacts with GSLs and *chc-1* but not with AP-1/*aps-1* in polarity maintenance.

Development (2019) 146, dev174508. doi:10.1242/dev.174508

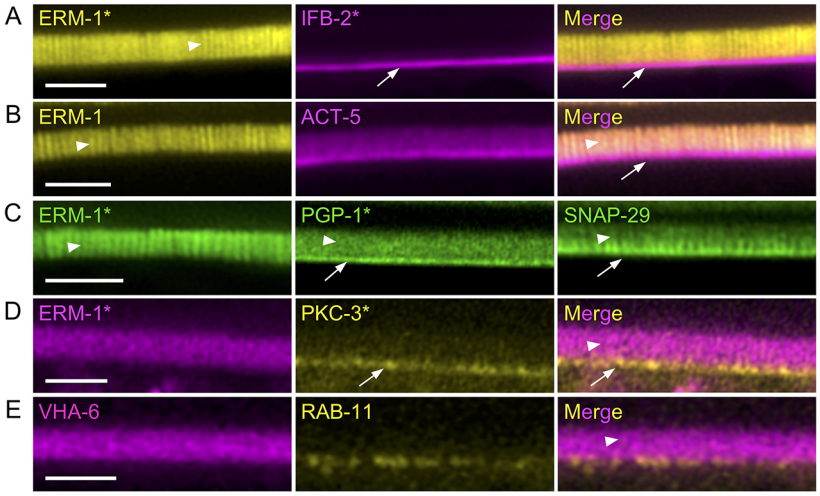

Fig. 4. Super-resolution imaging of the intestinal apical PM. (A-E) Adult worm strains expressing the indicated markers were mounted and imaged. Asterisks indicate endogenously tagged markers, whereas arrowheads and arrows indicate microvilli and presumptive terminal webs/endotubes, respectively. Merge channels allow the visualization of the colocalization between ERM-1 and ACT-5 in microvilli (B). Scale bars: 2 µm.

V0-ATPase silencing phenocopies microvillus inclusion disease

Next, we asked whether the polarity defects associated with V0-ATPase silencing were associated with brush border structural defects. Combined TEM and super-resolution imaging demonstrated that prolonged V0-ATPase silencing [72 and 96 h of V0/*vha-1*(*RNAi*)] specifically induced microvillus atrophy, with smaller, thinner or even absent microvilli at the apical PM of enterocytes (Fig. 6A-C and Fig. S5A). Conversely, V1/*vha-8*(*RNAi*), despite inducing a decreased worm size and a mild decrease in microvilli length, did not affect microvilli structure and organization (Fig. 6A-C and Fig. S5B). The severe apical PM defect induced by V0/*vha-1* silencing was observed along the whole surface of the lumen and was often associated with luminal dilatation and a local unhooking of the microvilli membrane from the underlying cytoskeleton (Fig. 6A and Fig. S5C) as well as slightly lengthened adherens junctions (CeAJs) (Fig. S5D,E). However, we could not resolve significant defects in the terminal web/endotube upon V0/*vha-1* or V1-ATPase/*vha-8* by TEM (Fig. 6A and Fig. S6A) or by analyzing the apical localization of the endotube marker IFB-2 (Bossinger et al., 2004) (Fig. 6D,E). Notably, IFB-2 was not basolaterally mislocalized with ERM-1 upon V0-ATPase/*vha-1*(*RNAi*) (Fig. 6E). Thus, V0/*vha-1* knockdown specifically led to severe apical PM structural defects, which could affect the apical localization of brush border, PAR modules and other proteins, which would result in defective absorptive function of the enterocytes, in line with the luminal accumulation of cellular or bacterial debris and the absence of yolk storage granules observed in V0/*vha-1*(*RNAi*) but not V1/*vha-8*(*RNAi*) worms (Fig. S5F,G).

Surprisingly, prolonged V0/*vha-1* silencing led to the accumulation of rounded ERM-1^{+} and ACT-5^{+} structures

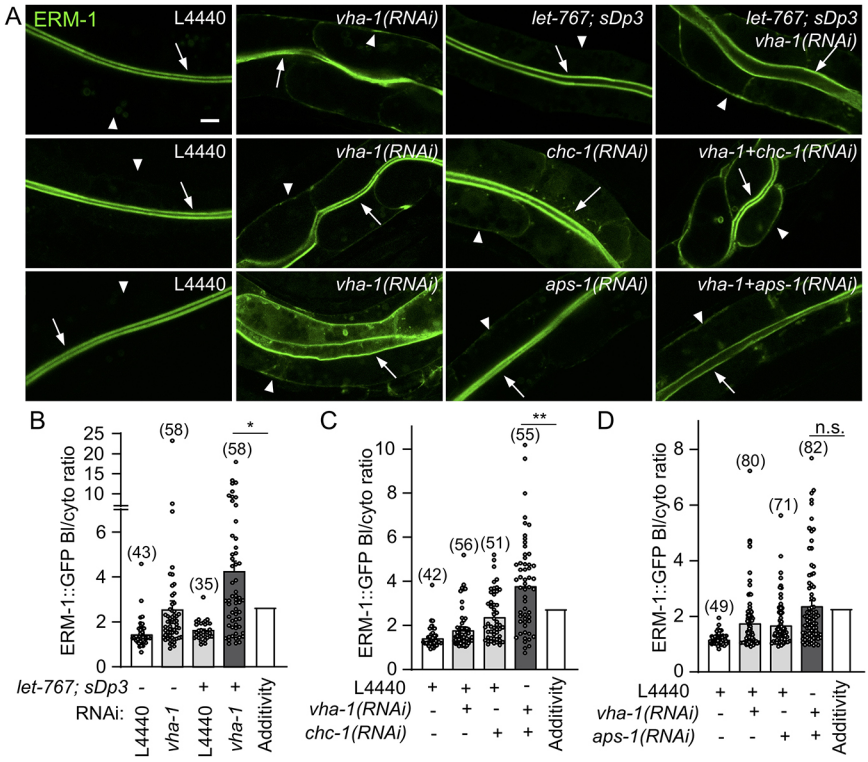

Fig. 5. V0-ATPase interacts genetically with GSLs and clathrin/*chc-1* in intestinal polarity maintenance. (A) ERM-1::GFP-expressing control or *let-767;sDp3* worms were silenced for control (L4440) or a mix of control (L4440), *vha-1*, *chc-1* or *aps-1* RNAi as indicated, and then imaged. (B-D) The quantification of the ERM-1::GFP basolateral/cytoplasmic ratio. Histograms are mean±s.e.m. on each panel, dots represent individual worms and the total number of worms from three (B-C) or four (D) independent experiments is indicated in brackets. 'Additivity' shows the sum of individual knockdowns or mutants. A specific statistical analysis was used to test the significance of the difference between double loss-of-function and additivity (see Materials and Methods). Arrows and arrowheads show the apical and basolateral PM, respectively. In all micrographs, worms are at the L4/young adult developmental stage. Scale bar: 5 µm. n.s. nonsignificant, *P<0.05, **P<0.01.

Development (2019) 146, dev174508. doi:10.1242/dev.174508

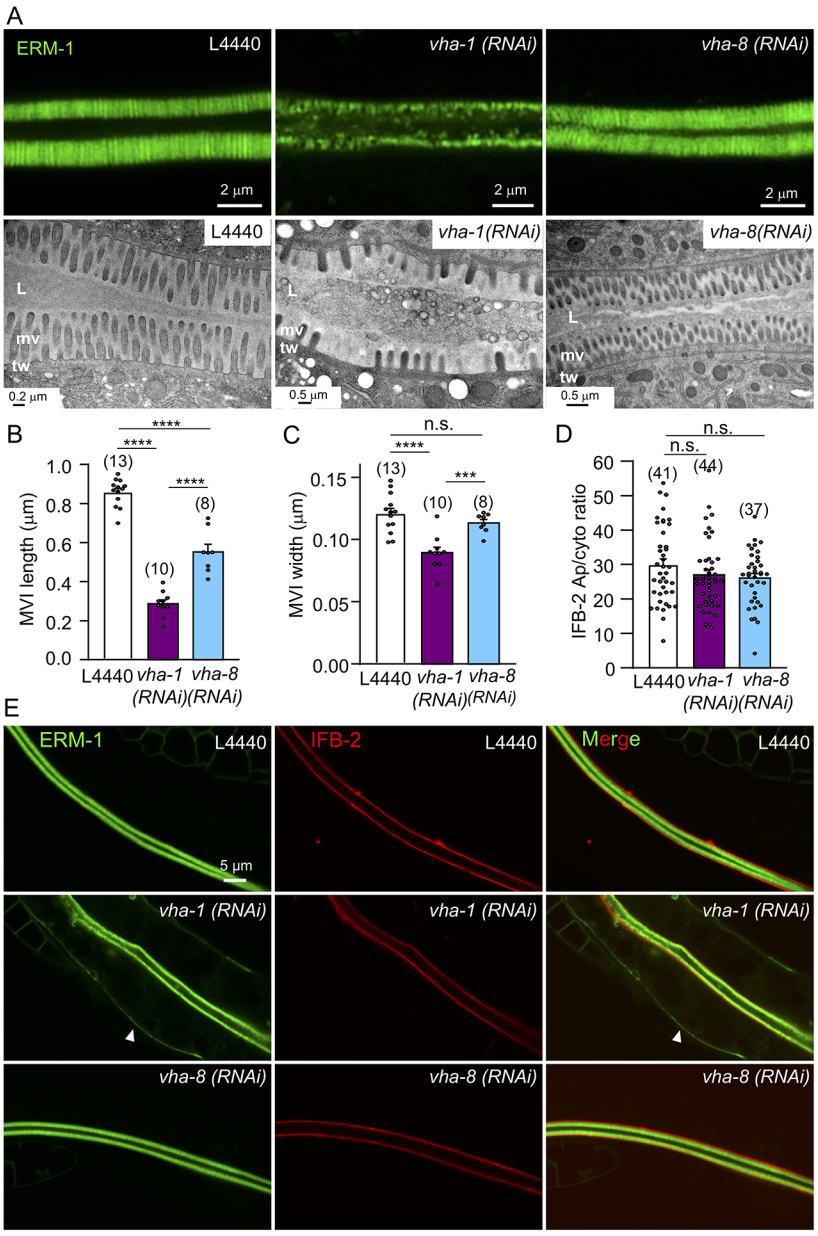

Fig. 6. V0-ATPase silencing induces microvillus atrophy in *C. elegans*. (A) Visualization of microvilli by super-resolution (upper panels, 96 h RNAi, ERM-1::GFP) and TEM (lower panels, 72 h RNAi) analysis. Control animals showed the typical intestinal brush border morphology consisting of a dense array of microvilli surrounded by a glycocalyx and stabilized by the terminal web/endotube. Conversely, V0/*vha-1*(*RNAi*) worms display a microvillus atrophy, with irregular, shorter and sparse microvilli, a phenotype that is not observed in V1/*vha-8*-depleted worms. The terminal web/endotube appears normal in all cases. L, lumen; mv, microvilli; tw, terminal web/endotube. (B-C) Measurement of microvilli length (B) and width (C) upon 72 h V0 and V1-ATPase knockdown from TEM images. Data are mean±s.e.m., *n*=5 microvilli/worm for the number of worms indicated in brackets. (D-E) Effect of V-ATPase silencing on the endotube component IFB-2. V0/*vha-1* or V1/*vha-8* were silenced in a strain co-expressing endogenously tagged ERM-1::mNG and IFB-2::wSc for 72 h and then imaged. Arrowheads show the basolateral mislocalization of ERM-1. (D) The quantification of the apical/cytoplasmic ratio of IFB-2. Histograms are mean ±s.e.m., dots represent individual worms and the total number of worms from two independent experiments is indicated in brackets. In micrographs, worms are at the L4/young adult (72 h RNAi) or adult (96 h RNAi) developmental stage. Scale bars: 0.2 µm or 0.5 µm in A; 5 µm in E. n.s., nonsignificant, ***P<0.001, ****P<0.0001.

(Fig. 7A,B), which displayed a microvilli-like pattern (Fig. 7C) and closely resembled cytoplasmic microvillus inclusions (MVIs) observed in patients with MVID (Iancu et al., 2007) and in a *STXBP2*-KO organoid MVID model (Mosa et al., 2018). These structures are also enriched in PKC-3 and SNAP-29 (Fig. 7D,E). TEM experiments performed on V0/*vha-1*-depleted worms confirmed the presence of typical MVIs lined by inward-pointing microvilli and an endotube (Fig. 7F). We also observed many vacuole-like structures which were heterogeneous in size (0.1-0.6 µm in diameter), shape and electron-density, and contained cellular material (Fig. 7G). These vacuole-like structures were positive for the microvilli-specific activated phospho-form of ezrin but not for the endotube marker IFB-2, as observed by immuno-electron microscopy (EM) (Fig. 7H and S6B) and were similar to the already-described 'irregular' MVIs that are probably immature or degrading MVIs (Iancu et al., 2007; Mosa et al., 2018). Strikingly, microvillus atrophy and MVIs are cellular hallmarks of MVID, a congenital disorder of intestinal epithelial cells (Ruemmele et al., 2006) caused by mutations in the genes encoding the trafficking proteins MYO5B (Müller et al., 2008), STX3 (Wiegerinck et al., 2014) or STXBP2 (Vogel et al., 2017b). Notably, enterocytes of patients with MVID also display similar polarity defects to those observed upon V0/*vha-1*(*RNAi*), such as the basolateral appearance of microvilli-specific proteins (Wiegerinck et al., 2014) and PAR polarity module components (Michaux et al., 2016) as well as the cytoplasmic displacement of trafficking proteins (i.e. STX3, the SNARE family component SNAP23 and cellubrevin; Dhekne et al., 2018). Finally, MVID has also been associated with enlarged lysosomes displaying a heterogeneous content and with the accumulation of cytoplasmic translucent vesicles (Iancu et al., 2007; Vogel et al., 2016) as well as the specific disorganization of $Rab11^{+}$ apical recycling endosomes (Vogel et al., 2017a; Talmon et al., 2012), which we also found in V0-ATPase knocked-down worms (Fig. 2). Together with the fact that *snap-29*(*RNAi*) also induces polarity and trafficking defects (Fig. 3D-G) and the formation of MVIs (Fig. 7I), these observations suggest that V0-

Development (2019) 146, dev174508. doi:10.1242/dev.174508

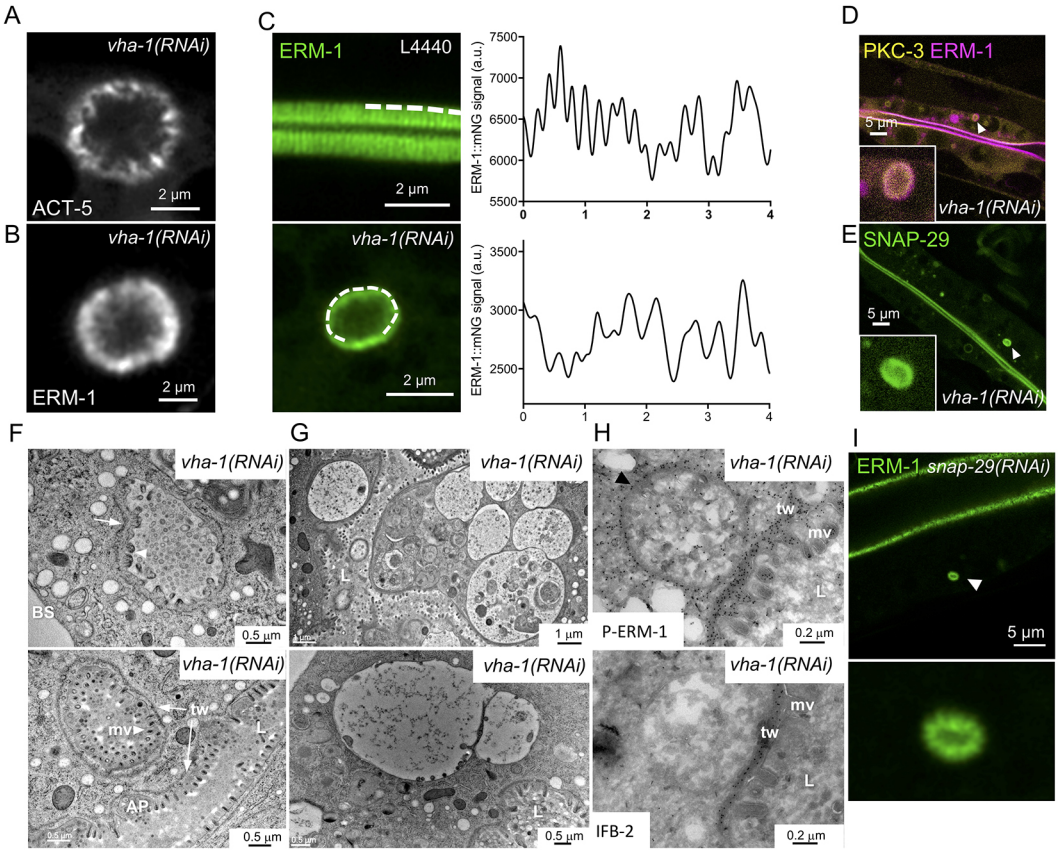

Fig. 7. V0-ATPase silencing induces MVID in *C. elegans*. (A,B) 96-h V0/*vha-1*(*RNAi*) induced the formation of cytoplasmic ACT-5^{+} and ERM-1^{+} microvillus inclusion-like structures, observed by super-resolution imaging. (C) Line scan on super-resolution images shows that rounded structures found in the cytoplasm (lower panel) displayed a periodic pattern reminiscent of apical microvilli (upper panel). A line scan of 4 µm was performed (dotted line) on ERM-1::mNG endogenously expressed at the level of the apical PM (control worms) and on ERM-1::mNG^{+} MVI-like structures [96 h of V0/*vha-1*(*RNAi*)]. (D,E) GFP::PKC-3 and GFP::SNAP-29 localized to V0/*vha-1*(*RNAi*)-induced MVI-like structures. Insert is a magnified image of the structure indicated by the arrowhead. (F-H) V0-ATPase silencing mainly induced cytoplasmic ERM-1^{+} vacuoles/irregular MVIs as well as typical MVIs. (F) Ultrastructural analysis by TEM of bona fide cytoplasmic inclusions observed in *C. elegans* silenced for V0/*vha-1* for 96 h. Note the classical MVIs showing the symmetrical, mainly inward-pointing arrangement of microvilli (arrowheads) and the area around the inclusion corresponding to the endotube (arrows). Typical MVIs were found in 3/16 worms. (G) Numerous and larger 'irregular' vacuole inclusions with a wide heterogeneity in size, shape and electron density were found after 96-h V0/*vha-1* silencing. The lumen contains probably amorphous, microvesicular, membranous and lipid components. (H) Immuno-EM analysis of the same vacuole-like structure using phospho-ezrin (upper panel) and IFB-2 (lower panel) antibodies and protein A gold in V0/*vha-1*(*RNAi*) worms (96 h) (dark dots). Both anti-phospho-ezrin and IFB-2 antibodies accumulated at the apical PM but only anti-phospho-ezrin also localized to V0/*vha-1*(*RNAi*)-induced vacuole-like structures. (I) *snap-29*(*RNAi*) (96 h) also induced the formation of cytoplasmic ERM-1::mNG^{+} MVIs, as observed by super-resolution imaging. Lower panel is a magnified picture of the MVI indicated by the arrowhead. In all micrographs, worms are at the adult developmental stage. L, lumen; mv, microvilli; tw, terminal web/endotube; AP, apical PM; BS, basal PM. Scale bars: 2 µm in A-C; 5 µm in D,E,I; 0.5 µm in F,G (lower panel); 1 µm in G (upper panel); 0.2 µm in H.

ATPase silencing in *C. elegans* fully recapitulates the defects observed in the enterocytes of patients with MVID and in MVID *in vitro* mammalian models (Table S3).

Study of MVI dynamics in a *C. elegans* model

Using live microscopy in intestinal organoids derived from *STXBP2* KO mice, we recently showed that MVIs can arise *de novo* in the cytoplasm or by internalization of both the apical and the basolateral PM (Mosa et al., 2018). To test whether these various modes of MVI onset are conserved in *C. elegans* upon V0-ATPase silencing, we performed live imaging on endogenously expressed ERM-1::mNG after 96 h of V0/*vha-1*(*RNAi*). This experiment confirmed that MVI-like structures rapidly nucleated in the cytoplasm (~3 min) and remained in the cytoplasm for <3 min to >1 h (Fig. 8A and Movies 1,2), a process that might involve lysosomal remodeling (Mosa et al., 2018). These structures might also arise by internalization of large ERM-1::GFP^{+} structures from the apical and basolateral PM of V0/*vha-1*-depleted worms (Fig. 8B, Fig. S6C and Movie 3), which has been linked to an autophagocytic process (Reinshagen et al., 2002). Given that autophagosomes and lysosomes have been linked to MVIs, we hypothesized that these structures undergo a cytoplasmic elimination through these degradation pathways. Consistently, live tracking of MVIs in *STXBP2* KO organoids reveals that MVIs are often surrounded by LAMP2^{+} membranes and mostly disappear by cytoplasmic disintegration, whereas the rest are eliminated by PM fusion or cell shedding (Mosa et al., 2018). Interestingly, we found that irregular MVIs induced by V0/*vha-1*(*RNAi*) were often in close proximity to mixed organelles/lysosomes (Fig. 8C) and that some ERM-1^{+} MVIs were also positive for the lysosomal marker LMP-1 (Fig. 8D). Furthermore, some MVIs were also surrounded by a second membranous layer positive for ERM-1 (Fig. 8E). Considering that: (1) ezrin accumulates at the phagosome membrane and regulates phagolysosomal fusion (Marion et al., 2011); and (2) V0-ATPase extinction dramatically activates autophagy, as ascertained by the relocalization of LGG-1::GFP

Development (2019) 146, dev174508. doi:10.1242/dev.174508

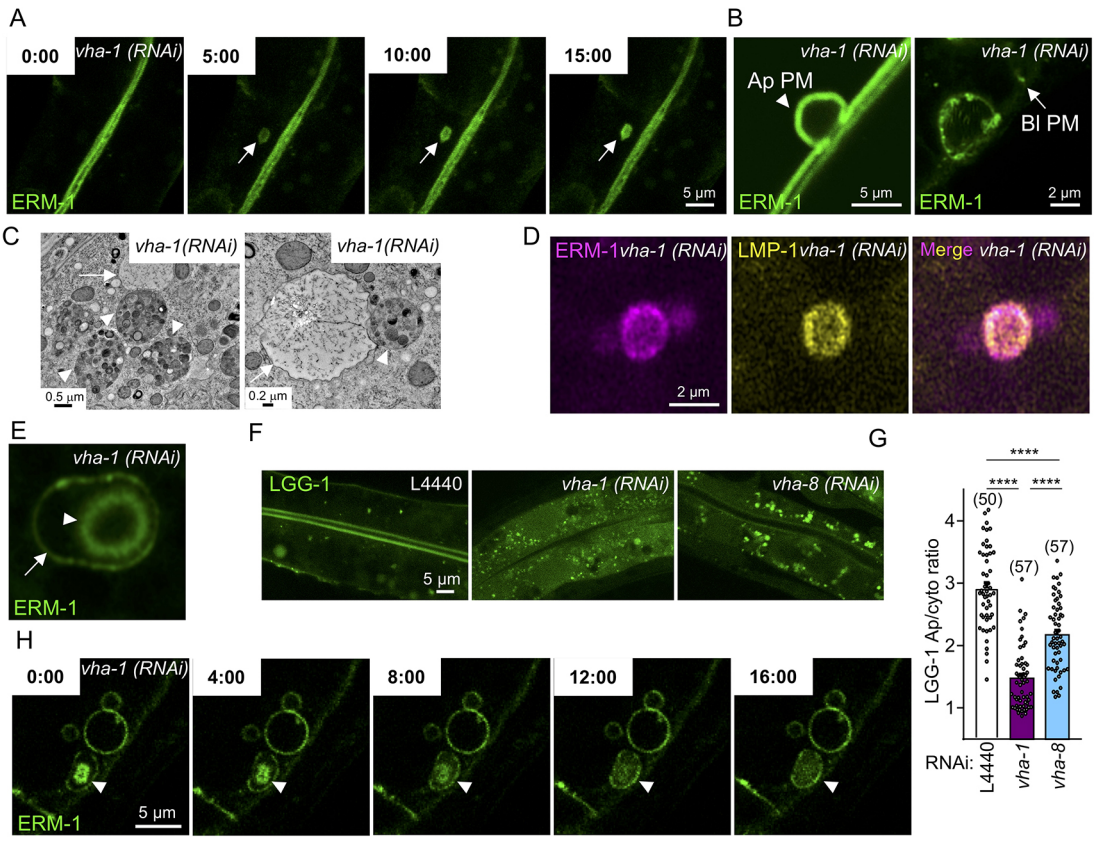

Fig. 8. Dynamics of microvillus inclusions in *C. elegans*. (A) MVI cytoplasmic nucleation observed by time-lapse super-resolution imaging in endogenous ERM-1::mNG-expressing worms silenced for V0/*vha-1* for 96 h. Snapshots are shown for every 5 min, MVI is indicated by the arrow. (B) MVIs can arise by internalization of the apical or basolateral PM. ERM-1::GFP-expressing worms were silenced for V0/*vha-1* for 72 h and imaged by conventional (left panel) or super-resolution (right panel) microscopy. Arrowhead and arrow show the apical and basolateral PM, respectively. (C) Irregular MVIs/vacuoles (arrows) were often in the vicinity of lysosomes/mixed organelles (arrowheads). N2 worms were silenced for V0/*vha-1* for 96 h and analyzed by TEM. (D) ERM-1::wSc and LMP-1::GFP colocalized at V0/*vha-1*(*RNAi*)-induced MVIs (96 h), as observed by super-resolution imaging. (E) 96 h V0/*vha-1*(*RNAi*)-induced MVIs (arrowhead) could be surrounded by a second ERM-1^{+} layer (arrow), observed by super-resolution imaging. (F-G) Autophagy was activated more upon V0/*vha-1*(*RNAi*) than V1/*vha-8*(*RNAi*). GFP::LGG-1-expressing worms were silenced for V0/*vha-1* or V1/*vha-8* for 72 h and then imaged. (G) The quantification of the GFP::LGG-1 apical/cytoplasmic ratio. Histograms are mean±s.e.m. on each panel, dots represent individual worms and the total number of worms from three independent experiments is indicated in brackets. ****P<0.0001. (H) Time-lapse super-resolution imaging of V0/*vha-1*(*RNAi*)-induced MVI disappearance (images taken every 4 min). In micrographs, worms are at the L4/young adult (72 h RNAi) or adult (96 h RNAi) developmental stage. Scale bars: 0.2 µm in C (right panel); 0.5 µm in C (left panel); 2 µm in B (right panel); 5 µm in A,B (left panel),F,H.

(LC3 *C. elegans* ortholog) from the apical PM to cytoplasmic puncta (Fig. 8F,G) (Chang et al., 2017), these data suggest that MVIs are eliminated by autophagosomes and/or lysosomes in the *C. elegans* intestine, as proposed in mammals. This was confirmed by time-lapse microscopy on ERM-1^{+} MVIs, which progressively disintegrated in the cytoplasm or inside ERM-1^{+} secondary structures (Fig. 8H and Movie 4).

DISCUSSION

By performing a double-RNAi screen in the *C. elegans* intestine, we identified a new function of the V0-ATPase complex in the maintenance of one of the most prominent cell surfaces, the absorptive apical PM of enterocytes. Our results demonstrate that V0-ATPase ensures the apical localization of polarity modules, brush border components and trafficking factors, a major role that is substantiated by the severe brush border defects resulting from V0/*vha-1* silencing. This study confirms the biological significance of systematic RNAi screens in *C. elegans* to understand the complex mechanisms of polarity maintenance. Indeed, this model has enabled researchers to characterize the major role of membrane trafficking factors in epithelial polarity maintenance, including GSLs (Zhang et al., 2011), clathrin and its adaptor AP-1 (Shafaq-Zadah et al., 2012; Zhang et al., 2012), the kinase Lats/WTS-1 (Kang et al., 2009) and the interactions between polarity proteins and membrane trafficking (Winter et al., 2012; Balklava et al., 2007).

Intriguingly, whereas interfering with the clathrin/AP-1, PAR-5 or GSL pathways induced a RAB-11^{+} endosomes loss and an inversion of both apical and basolateral PM protein polarity (Shafaq-Zadah et al., 2012; Zhang et al., 2012, 2011; Winter et al., 2012), we showed here that V0/*vha-1* silencing had a specific effect on brush border and CDC-42/PAR polarity but not on transmembrane or basolateral proteins (Fig. 1 and Figs S1I,J and S3A,B). This surprising result points to a specific role of V0-ATPase in late trafficking events, downstream of GSLs (Zhang et al., 2011, 2012), clathrin and AP-1 (Shafaq-Zadah et al., 2012; Zhang et al., 2012) or Lats/WTS-1 (Kang et al., 2009), which might control earlier sorting events (Fig. S7). This conclusion is supported by: (1) the deleterious effect of GSL biosynthesis enzymes, *chc-1* or *aps-1* silencing on the apical localization of the V0-ATPase subunit VHA-6 (Zhu et al., 2015); (2) the known function of V0-ATPase in vesicle fusion to the PM and its localization in microvilli; (3) the accumulation of vesicles upon V0/*vha-1* silencing; (4) the role of

Development (2019) 146, dev174508. doi:10.1242/dev.174508

SNAP-29 downstream of V0-ATPase; and (5) the phenotypic similarities with the loss of MYO5B, STX3 or STXBP2 in patients with MIVD, which all control late trafficking events just upstream of, or during fusion to, the apical PM.

Furthermore, this model is also consistent with the genetic interaction experiments performed in this study, which advocated that the clathrin/AP-1 and GSL sorting pathways converge towards RAB-11$^+$ endosomes and V0-ATPase to ensure the polarized localization of soluble factors necessary for intestinal polarity maintenance (i.e. the PAR module and ERM-1). First, AP-1 could regulate an early sorting step that might rely on the recognition of sorting signals in cargo protein sequences, as shown previously for AP-1-dependent basolateral sorting through di-leucin or tyrosine-based motifs (Bonifacino, 2014); the additional effect following the loss of AP-1 and V0-ATPase suggests that the latter controls an AP-1-independent pathway or at least more than just AP-1-dependent cargos. Second, GSLs could control a parallel early sorting step based on other signals (i.e. GPI anchor) in a pathway also encompassing V0-ATPase-dependent apical PM exocytosis, based on the synthetic effect observed. Hence, we propose that polarity module and brush border components undergo a complex apical PM targeting mechanism involving various endosomal trafficking steps along the secretory and endocytic recycling pathways, among which V0-ATPase controls a crucial step necessary for their apical polarity.

The precise mechanism by which V0-ATPase controls the maintenance of the intestinal polarity remains to be elucidated. The most-studied function of this complex in membrane trafficking relies on the H^+-pump-dependent (V0+V1 subunits) acidification of intracellular organelles, which ensures their maturation and transport capacity (Maxson and Grinstein, 2014). Here, we confirmed that inhibition of this function by inhibiting *vha-8* expression affected endosomal organization (Fig. 2 and Fig. S2) as well as the apical confinement of the polarity module components CDC-42, PAR-6 and PKC-3 (Figs 1 and S1), but has no effect on the polarized localization of these factors or ERM-1, or on the structure of the apical PM (Table S2). This suggests that trafficking events dependent on V-ATPase activity are required to ensure the confinement of these proteins at the apical PM, probably through the targeting of scaffold proteins. However, our results demonstrated a specific requirement for its V0 sector in polarity maintenance, in an acidification-independent manner and probably through its already-characterized function in vesicle exocytosis (Hiesinger et al., 2005; Di Giovanni et al., 2010; Baars et al., 2007; Liégeois et al., 2006). Indeed, the functional relevance of V0-ATPase interaction with the fusion machinery has been demonstrated in many species, such as *Drosophila* or *Torpedo marmorata*, where the V0-a1 subunit (V100 in *Drosophila*) has been shown to interact with the t-SNAREs Syx and SNAP25 (Hiesinger et al., 2005) and with the v-SNARE VAMP-2 (Morel et al., 2003), respectively. Furthermore, the direct interaction between the V0-c subunit (the ortholog of *vha-1*) and VAMP2 has been shown to be indispensable for efficient synaptic vesicle fusion in mammalian cells (Di Giovanni et al., 2010). A similar mechanism could occur for the apical exocytosis of vesicles containing polarity and brush border components, which might directly interact with the V0-ATPase, and/or apical adaptor proteins, such as the ezrin partner NHERF-1/EBP50, which was recently found in interactome studies to associate with the V-ATPase (Merkulova et al., 2015). In line with this, we found that V0/*vha-1*(*RNAi*) decreased the apical confinement of SNAP-29, a member of the SNAP23/25/29 family (Steegmaier et al., 1998), which is mislocalized in MVID mammalian models (Dhekne et al., 2018), and that *snap-29* extinction phenocopies that of V0/*vha-1* on *C. elegans* intestinal polarity. Given that SNAP-29 has been localized to RAB-11$^+$ endosomes in *C. elegans* (Kang et al., 2011), probably at the terminal web (Fig. 4), and that mammalian SNAP29 physically interacts with STX3 (Steegmaier et al., 1998), V0-ATPase could directly interact with SNAP-29 to target the exocytosis of RAB-11$^+$ endosomes and be involved in the same pathway as MYO5B, STX3 or STXBP2. Why disruption of a late fusion event downstream of RAB-11$^+$ endosomes induced such a dramatic loss of these organelles remains to be elucidated. Consistent with our TEM data (Fig. 2), it is plausible that recycling endosomes spread into vesicles that are no longer associated with RAB-11.

Beyond disturbing polarity, we also found that V0/*vha-1* silencing induced severe microvilli defects and the formation of MVIs that are typical features of MVID. MVID is a devastating orphan congenital disorder of intestinal cells that manifests as intractable diarrhea and intestinal absorption defects appearing in neonatal babies (Halac et al., 2011; Ruemmele et al., 2006); current therapeutic avenues rely on total parenteral nutrition or small bowel transplantation (Halac et al., 2011). MVID originates from mutations of MYO5B, STX3 or STXBP2 (Dhekne et al., 2018), which belong to the same apical trafficking pathway. At the molecular level, a defective apical PM tethering of RAB-8$^+$/RAB-11$^+$ endosomes by the molecular motor MYO5B (Knowles et al., 2014), which interacts with STX3 (Vogel et al., 2015) in concert with STXBP2, which has an accessory role in STX3-dependent vesicle tethering (Vogel et al., 2017b), has been proposed to be the major pathway leading to the MVID phenotype. Hence, MVID is strictly linked to a polarized trafficking defect and *in vitro* mammalian 2D or 3D cell culture models have been developed to study its currently ill-defined underlying mechanisms, based on MYO5B or Rab8/Rab11 silencing and disruption of MYO5B-Rab8/11 interactions (Feng et al., 2017; Knowles et al., 2014; Engevik et al., 2018; Kravtsov et al., 2016; Weis et al., 2016; Vogel et al., 2015; Schneeberger et al., 2015) as well as STX3 (Wiegerinck et al., 2014; Vogel et al., 2015) or STXBP2 (Mosa et al., 2018; Vogel et al., 2017b) mutations.

However, some discrepancies were found while trying to integrate polarity maintenance mechanisms identified *in vitro* and *in vivo*. For instance, whereas AP-1 is renowned for basolateral sorting in cultured cells (Gravotta et al., 2012), its crucial role in apical trafficking has been characterized *in vivo* in *C. elegans* and in mouse (Shafaq-Zadah et al., 2012; Zhang et al., 2012; Hase et al., 2013). Whereas the *in vitro* culture of intestinal organoids derived from patients with MVID or mice deficient in genes causing MVID (Schneeberger et al., 2018; Mosa et al., 2018; Wiegerinck et al., 2014) and the mutation of *myoVb*/*goosepimples* in zebrafish (Sidhaye et al., 2016) appear to reproduce most of the cellular and structural hallmarks of MVID, these models are not suitable for systematic studies. Conversely, the *in vivo*, easy-to-use and screening-amenable *C. elegans* model has been widely used to understand intestinal polarity mechanisms; however, single deletion of the orthologs of MVID-causing genes (i.e. *hum-2*/*MYO5B* and *unc-64*/*STX3*) does not induce an MVID phenotype (A.B.-M and G.M., unpublished), probably because of compensatory mechanisms. We describe here for the first time a *C. elegans* model, V0-ATPase silencing, which fully phenocopies the hallmarks of MVID (Table S3) and that could be used to better characterize polarity maintenance mechanisms and MVID pathophysiology. As a proof of principle, we studied the

Development (2019) 146, dev174508. doi:10.1242/dev.174508

dynamics of MVIs, the onset and elimination of which remain enigmatic. According to the 'combined' model of MVI onset (Schneeberger et al., 2018), the results of a recent paper using *STXBP2* KO organoids (Mosa et al., 2018) and the results of the present study (Fig. 7), we showed that MVIs might arise by two main mechanisms: *de novo* nucleation in the cytoplasm or internalization of the PM. Both might rely on the failure of apical exocytosis from RAB-11$^+$ endosomes. Indeed, this defect would, on the one hand, result in the sequestration of polarity factors in the cytoplasm, which might be an upstream signal to target newly synthesized apical PAR, PM proteins and cytoskeleton and, consequently, nucleate a new apical PM in the cytoplasm on accumulating vesicles. On the other hand, defective exocytosis might lead to a local apical PM protein and/or lipid homeostasis defect that would create a signal for endocytosis and targeting for autophagosomal-lysosomal degradation, as proposed previously (Reinshagen et al., 2002) and verified in this report (Fig. 8). Finally, our data suggest that V0-ATPase is involved in the etiology of MVID and other absorption disorders associated with apical PM defects or affected in patients (Table S3). Complementary use of both *C. elegans*, as a tool to screen for correctors of polarity maintenance defects, as well as mammalian intestinal organoids or human samples to confirm the conservation of V0-ATPase function, could lead to a better understanding of the mechanisms of polarity maintenance as well as that of rare genetic enteropathies.

MATERIALS AND METHODS

C. elegans strains and maintenance

Strains were maintained under typical conditions as described previously (Brenner, 1974). CRISPR/CAS9-genome-edited mNG and mScarlet-tagged ERM-1, IFB-2, UNC-64 and PGP-1 were generated at the Biologie de *Cænorhabditis elegans* facility (UMS3421, Lyon, France). The strains used in this study are listed in Table S4.

Gene silencing and screening by RNAi

Larval RNAi was performed by feeding using the Ahringer-Source BioScience library, as previously described (Kamath and Ahringer, 2003; Shafaq-Zadah et al., 2012). Briefly, adult hermaphrodites were bleached and transferred to RNAi plates containing HT115 *Escherichia coli* expressing the L4440 plasmid alone (control) or encoding the RNAi. For co-silencing of V0/*vha-1* and *chc-1*/*aps-1*, equal amounts of exponential phase bacterial culture (OD_{600} ~0.6) were mixed either together or with L4440 (single silencing). Developing worms were kept in RNAi for 72-96 h before mounting and imaging. RNAi specificity was verified by sequencing and efficiency by target::GFP signal disappearance, as shown in Figs S1-S4 and S6.

In vivo confocal imaging using *C. elegans*

C. elegans imaging was performed *in vivo* by mounting the worms on a 10% agarose pad in a solution of 100 nm polystyrene microbeads (Polysciences Inc.) to stop any worm movement. Confocal observations were performed on the anterior intestinal cells using a Leica (Wetzlar, Germany) SPE equipped with a 63×, 1.4 NA objective (LAS AF software) or a super-resolution Zeiss (Oberkochen, Germany) LSM880+Airyscan equipped with a 63×, 1.4 NA objective (Zen Black software). All images were examined using Fiji software (imagej.net/Fiji).

TEM

Control and RNAi worms (72-96 h) were fixed by high-pressure freezing with EMPACT-2 (Leica Microsystems) and then freeze substituted in anhydrous acetone containing 1% OsO4, 0.5% glutaraldehyde and 0.25% uranyl acetate for 60 h in a freeze substitution system (AFS-2, Leica Microsystems). Larvae were embedded in Epon-Araldite mix (EMS hard formula). Adhesive frames were used (11560294 GENE-FRAME 65 µl, Thermo Fisher Scientific) for flat-embedding, as previously described (Kolotuev et al., 2012), to gain better anteroposterior orientation and sectioning. Ultrathin sections were cut on an ultramicrotome (UC7; Leica Microsystems) and collected on formvar-coated slot grids (FCF2010-CU, EMS). Each larva was sectioned in five different places with ≥10 µm between each grid to ensure that different cells were observed. Each grid contained at least ten consecutive sections of 70 nm. TEM grids were observed using a JEM-1400 transmission electron microscope (JEOL) operated at 120 kV, equipped with a Gatan Orius SC 1000 camera (Gatan) and piloted by the Digital Micrograph program. Micrographs were analyzed using Fiji software.

Immuno-EM

Immuno-EM was performed as previously described (Nicolle et al., 2015). Briefly, for ultrathin cryosections and immunogold labeling, larvae were fixed with 4% paraformaldehyde plus 0.1% glutaraldehyde in M9 buffer. Worms were embedded in 12% gelatin and infused in 2.3 M sucrose. Gelatin blocks were frozen and processed for ultracryomicrotomy (UC7cryo; Leica Microsystems). Ultrathin cryosections (80 nm) were double-immunogold labeled and analyzed by TEM, as described earlier. We applied primary antibodies [rabbit anti-phospho-ezrin (Thr567)/radixin (Thr564)/moes (Thr558) (1:100, Cell Signaling Technology, 3726S), mouse anti-IFB-2 (1:10, DSHB, MH33) or mouse anti-actin (1:50, Cedarlane Laboratories, CLT9001)] detected using protein A conjugated to 10-nm gold particles (1:50, CMC, PAG).

Immunostaining

Embryos were collected in a 10µl drop of M9 on a microscope slide and covered with a coverslip for 90 sec. Then, the slide was plunged in liquid N_2 for 10 sec and the coverslip was removed sharply. The embryos were then further fixed in methanol for 20 min at −20°C (freeze-crack-methanol method). After washing in 1× PBS, the embryos were stained for P-ERM-1 [rabbit anti-phospho-ezrin (Thr567)/radixin (Thr564)/moes (Thr558); 1:300] and IFB-2 (mouse anti-IFB-2; 1:50) in 1× PBS, 0.2% Tween, 1% bovine serum albumin overnight at 4°C. After two washes in 1× PBS-0.2% Tween, they were incubated with anti-rabbit A532 and anti-mouse A633 (1:500, Invitrogen) secondary antibodies in blocking solution for 1 h at room temperature. After further washes, the slides were mounted in Mowiol.

Quantification

The apical/cytoplasmic ratio of all markers and the basolateral/cytoplasmic ratio of SLCF-1 and SYX-1 were calculated by quantifying the signal intensity on a line covering the width of the PM and covering at least the length of two adjacent intestinal cells. The intensity of the same line was quantified in the cytoplasm underneath the PM. Basolateral ERM-1 appearance was calculated using the Plot Profile function of Fiji, with a region of interest (ROI) of 1.3 µm long crossing the highest basolateral PM intensity. The five highest values were divided by the mean fluorescence of the same ROI in the cytoplasm. Microvilli length and width were quantified using Fiji on TEM pictures of at least five sections per worm. The number of RAB-5$^+$ vesicles was quantified using a home-made plugin for Fiji, as described elsewhere (Gillard et al., 2015).

Statistical analysis

Results are presented as mean±s.e.m. of the number of independent experiments indicated in the legends, and scattered dots represent individual worms. The total number of larvae used is indicated in brackets on histograms. Unless specified, *P*-values were calculated with the means of at least three independent experiments by two-tailed unpaired Student's *t*-test and a 95% confidence level was considered significant. Normal distribution of data and homogeneity of variance were validated by calculating the skew factor (−2>skew<2) and the *F*-test, respectively. The Mann–Whitney *U*-test was used for calculating the *P*-values of non-normal distributions and Welch correction was applied to normal distributions with non-homogenous variances. Genetic interactions were calculated using a linear model including principal effects and the interaction effect. A permutation test was used to compute the *P*-values associated with the coefficients of the model, because normality assumptions were not met. This allowed us to determine the statistically significant interactions between V0-ATPase and clathrin or GSLs. Differences were significant at $p<0.05$.

Acknowledgements
We thank Verena Gobel, Barth Grant, Ken Kemphues, Jeremy Nance, Emily Troemel and Ken Sato for strains. We also thank Maïté Carre-Pierrat (Biologie de *Cænorhabditis elegans* facility, UMS3421, Lyon, France) who generated several of the CRISPR/Cas9 genome-edited strains used in this study. Some strains were provided by the CGC, which is funded by National Institutes of Health Office of Research Infrastructure Programs (P40 OD010440; University of Minnesota, USA). We thank Aurélien Perrin for the initial PAR-6::GFP screen, Raphaël Dima and Justine Cailloce for help with screen validation, as well as Anne Pacquelet for critical reading of the manuscript and helpful discussions. Imaging was performed at the photonic and electron microscopy facilities of the Microscopy Rennes Imaging Center (MRiC), Rennes, France.

Competing interests
The authors declare no competing or financial interests.

Author contributions
Conceptualization: A.B.-M., G.M.; Methodology: A.B.-M., O.N., M.H., Y.L.C.; Formal analysis: A.B.-M.; Investigation: A.B.-M., O.N., M.H.; Data curation: A.B.-M.; Writing - original draft: A.B.-M., G.M.; Writing - review & editing: A.B.-M., G.M.; Supervision: G.M.; Funding acquisition: G.M.

Funding
This work was supported by the Ligue contre le Cancer Grand Ouest (22/29/35/41/72) and the Fondation maladies rares (169608). We also receive institutional funding from the Centre national de la recherche scientifique (CNRS) and the Université de Rennes 1. A.B.-M. is the recipient of a postdoctoral fellowship from La Ligue Nationale Contre le Cancer (2017-2018) and this project has received funding from the European Union's Horizon 2020 research and innovation programme under the Marie Sklodowska-Curie grant agreement 844070.

Supplementary information
Supplementary information available online at
http://dev.biologists.org/lookup/doi/10.1242/dev.174508.supplemental

References

Allman, E., Johnson, D. and Nehrke, K. (2009). Loss of the apical V-ATPase a-subunit VHA-6 prevents acidification of the intestinal lumen during a rhythmic behavior in C. elegans. *Am. J. Physiol. Cell Physiol.* **297**, C1071-C1081. doi:10.1152/ajpcell.00284.2009

Baars, T. L., Petri, S., Peters, C. and Mayer, A. (2007). Role of the V-ATPase in regulation of the vacuolar fission-fusion equilibrium. *Mol. Biol. Cell* **18**, 3873-3882. doi:10.1091/mbc.e07-03-0205

Balklava, Z., Pant, S., Fares, H. and Grant, B. D. (2007). Genome-wide analysis identifies a general requirement for polarity proteins in endocytic traffic. *Nat. Cell Biol.* **9**, 1066-1073. doi:10.1038/ncb1627

Bonifacino, J. S. (2014). Adaptor proteins involved in polarized sorting. *J. Cell Biol.* **204**, 7-17. doi:10.1083/jcb.201310021

Bossinger, O., Fukushige, T., Claeys, M., Borgonie, G. and Mcghee, J. D. (2004). The apical disposition of the Caenorhabditis elegans intestinal terminal web is maintained by LET-413. *Dev. Biol.* **268**, 448-456. doi:10.1016/j.ydbio.2004.01.003

Brenner, S. (1974). The genetics of Caenorhabditis elegans. *Genetics* **77**, 71-94.

Bryant, D. M., Datta, A., Rodríguez-Fraticelli, A. E., Peränen, J., Martín-Belmonte, F. and Mostov, K. E. (2010). A molecular network for de novo generation of the apical surface and lumen. *Nat. Cell Biol.* **12**, 1035-1045. doi:10.1038/ncb2106

Chang, J. T., Kumsta, C., Hellman, A. B., Adams, L. M. and Hansen, M. (2017). Spatiotemporal regulation of autophagy during Caenorhabditis elegans aging. *eLife* **6**, e18459. doi:10.7554/eLife.18459

Collaco, A. M., Geibel, P., Lee, B. S., Geibel, J. P. and Ameen, N. A. (2013). Functional vacuolar ATPase (V-ATPase) proton pumps traffic to the enterocyte brush border membrane and require CFTR. *Am. J. Physiol. Cell Physiol.* **305**, C981-C996. doi:10.1152/ajpcell.00067.2013

Colombié, N., Choesmel-Cadamuro, V., Series, J., Emery, G., Wang, X. and Ramel, D. (2017). Non-autonomous role of Cdc42 in cell-cell communication during collective migration. *Dev. Biol.* **423**, 12-18. doi:10.1016/j.ydbio.2017.01.018

Crawley, S. W., Mooseker, M. S. and Tyska, M. J. (2014). Shaping the intestinal brush border. *J. Cell Biol.* **207**, 441-451. doi:10.1083/jcb.201407015

Desclozeaux, M., Venturato, J., Wylie, F. G., Kay, J. G., Joseph, S. R., Le, H. T. and Stow, J. L. (2008). Active Rab11 and functional recycling endosome are required for E-cadherin trafficking and lumen formation during epithelial morphogenesis. *Am. J. Physiol. Cell Physiol.* **295**, C545-C556. doi:10.1152/ajpcell.00097.2008

Dhekne, H. S., Hsiao, N.-H., Roelofs, P., Kumari, M., Slim, C. L., Rings, E. H. H. M. and van Ijzendoorn, S. C. D. (2014). Myosin Vb and Rab11a regulate phosphorylation of ezrin in enterocytes. *J. Cell Sci.* **127**, 1007-1017. doi:10.1242/jcs.137273

Dhekne, H. S., Pylypenko, O., Overeem, A. W., Ferreira, R. J., van der Velde, K. J., Rings, E. H. H. M., Posovszky, C., Swertz, M. A., Houdusse, A. and van IJzendoorn, S. C. D. (2018). MYO5b, STX3, and STXBP2 mutations reveal a common disease mechanism that unifies a subset of congenital diarrheal disorders: a mutation update. *Hum. Mutat.* **39**, 333-344. doi:10.1002/humu.23386

Di Giovanni, J., Boudkkazi, S., Mochida, S., Bialowas, A., Samari, N., Lévêque, C., Youssouf, F., Brechet, A., Iborra, C., Maulet, Y. et al. (2010). V-ATPase membrane sector associates with synaptobrevin to modulate neurotransmitter release. *Neuron* **67**, 268-279. doi:10.1016/j.neuron.2010.06.024

Engevik, A. C., Kaji, I., Engevik, M. A., Meyer, A. R., Weis, V. G., Goldstein, A., Hess, M. W., Muller, T., Koepsell, H., Dudeja, P. K. et al. (2018). Loss of MYO5B leads to reductions in Na(+) absorption with maintenance of CFTR-dependent Cl(−) secretion in enterocytes. *Gastroenterology* **155**, 1883-1897.e10. doi:10.1053/j.gastro.2018.08.025

Feng, Q., Bonder, E. M., Engevik, A. C., Zhang, L., Tyska, M. J., Goldenring, J. R. and Gao, N. (2017). Disruption of Rab8a and Rab11a causes formation of basolateral microvilli in neonatal enteropathy. *J. Cell Sci.* **130**, 2491-2505. doi:10.1242/jcs.201897

Forgac, M. (2007). Vacuolar ATPases: rotary proton pumps in physiology and pathophysiology. *Nat. Rev. Mol. Cell Biol.* **8**, 917-929. doi:10.1038/nrm2272

Gillard, G., Shafaq-Zadah, M., Nicolle, O., Damaj, R., Pécréaux, J. and Michaux, G. (2015). Control of E-cadherin apical localisation and morphogenesis by a SOAP-1/AP-1/clathrin pathway in C. elegans epidermal cells. *Development* **142**, 1684-1694. doi:10.1242/dev.118216

Gravotta, D., Carvajal-Gonzalez, J. M., Mattera, R., Deborde, S., Banfelder, J. R., Bonifacino, J. S. and Rodriguez-Boulan, E. (2012). The clathrin adaptor AP-1A mediates basolateral polarity. *Dev. Cell* **22**, 811-823. doi:10.1016/j.devcel.2012.02.004

Guo, B., Liang, Q., Li, L., Hu, Z., Wu, F., Zhang, P., Ma, Y., Zhao, B., Kovács, A. L., Zhang, Z. et al. (2014). O-GlcNAc-modification of SNAP-29 regulates autophagosome maturation. *Nat. Cell Biol.* **16**, 1215-1226. doi:10.1038/ncb3066

Halac, U., Lacaille, F., Joly, F., Hugot, J.-P., Talbotec, C., Colomb, V., Ruemmele, F. M. and Goulet, O. (2011). Microvillous inclusion disease: how to improve the prognosis of a severe congenital enterocyte disorder. *J. Pediatr. Gastroenterol. Nutr.* **52**, 460-465. doi:10.1097/MPG.0b013e3181fb4559

Hase, K., Nakatsu, F., Ohmae, M., Sugihara, K., Shioda, N., Takahashi, D., Obata, Y., Furusawa, Y., Fujimura, Y., Yamashita, T. et al. (2013). AP-1B-mediated protein sorting regulates polarity and proliferation of intestinal epithelial cells in mice. *Gastroenterology* **145**, 625-635. doi:10.1053/j.gastro.2013.05.013

Hegan, P. S., Giral, H., Levi, M. and Mooseker, M. S. (2012). Myosin VI is required for maintenance of brush border structure, composition, and membrane trafficking functions in the intestinal epithelial cell. *Cytoskeleton (Hoboken)* **69**, 235-251. doi:10.1002/cm.21018

Hein, Z., Schmidt, S., Zimmer, K.-P. and Naim, H. Y. (2011). The dual role of annexin II in targeting of brush border proteins and in intestinal cell polarity. *Differentiation* **81**, 243-252. doi:10.1016/j.diff.2011.01.009

Heintzelman, M. B. and Mooseker, M. S. (1990a). Assembly of the brush border cytoskeleton: changes in the distribution of microvillar core proteins during enterocyte differentiation in adult chicken intestine. *Cell Motil. Cytoskeleton* **15**, 12-22. doi:10.1002/cm.970150104

Heintzelman, M. B. and Mooseker, M. S. (1990b). Structural and compositional analysis of early stages in microvillus assembly in the enterocyte of the chick embryo. *Differentiation* **43**, 175-182. doi:10.1111/j.1432-0436.1990.tb00444.x

Hiesinger, P. R., Fayyazuddin, A., Mehta, S. Q., Rosenmund, T., Schulze, K. L., Zhai, R. G., Verstreken, P., Cao, Y., Zhou, Y., Kunz, J. et al. (2005). The v-ATPase V0 subunit a1 is required for a late step in synaptic vesicle exocytosis in Drosophila. *Cell* **121**, 607-620. doi:10.1016/j.cell.2005.03.012

Iancu, T. C., Mahajnah, M., Manov, I. and Shaoul, R. (2007). Microvillous inclusion disease: ultrastructural variability. *Ultrastruct. Pathol.* **31**, 173-188. doi:10.1080/01913120701350712

Ji, Y. J., Choi, K. Y., Song, H.-O., Park, B.-J., Yu, J.-R., Kagawa, H., Song, W. K. and Ahnn, J. (2006). VHA-8, the E subunit of V-ATPase, is essential for pH homeostasis and larval development in C. elegans. *FEBS Lett.* **580**, 3161-3166. doi:10.1016/j.febslet.2006.04.067

Kamath, R. S. and Ahringer, J. (2003). Genome-wide RNAi screening in Caenorhabditis elegans. *Methods* **30**, 313-321. doi:10.1016/S1046-2023(03)00050-1

Kang, J., Shin, D., Yu, J.-R. and Lee, J. (2009). Lats kinase is involved in the intestinal apical membrane integrity in the nematode Caenorhabditis elegans. *Development* **136**, 2705-2715. doi:10.1242/dev.035485

Kang, J., Bai, Z., Zegarek, M. H., Grant, B. D. and Lee, J. (2011). Essential roles of snap-29 in C. elegans. *Dev. Biol.* **355**, 77-88. doi:10.1016/j.ydbio.2011.04.013

Kiela, P. R. and Ghishan, F. K. (2016). Physiology of intestinal absorption and secretion. *Best Pract. Res. Clin. Gastroenterol.* **30**, 145-159. doi:10.1016/j.bpg.2016.02.007

Knight, A. J., Johnson, N. M. and Behm, C. A. (2012). VHA-19 is essential in Caenorhabditis elegans oocytes for embryogenesis and is involved in trafficking in oocytes. *PLoS ONE* **7**, e40317. doi:10.1371/journal.pone.0040317

Knowles, B. C., Roland, J. T., Krishnan, M., Tyska, M. J., Lapierre, L. A., Dickman, P. S., Goldenring, J. R. and Shub, M. D. (2014). Myosin Vb uncoupling from RAB8A and RAB11A elicits microvillus inclusion disease. *J. Clin. Invest.* **124**, 2947-2962. doi:10.1172/JCI71651

Kolotuev, I., Bumbarger, D. J., Labouesse, M. and Schwab, Y. (2012). Targeted ultramicrotomy: a valuable tool for correlated light and electron microscopy of small model organisms. *Methods Cell Biol.* **111**, 203-222. doi:10.1016/B978-0-12-416026-2.00011-X

Kravtsov, D. V., Ahsan, M. K., Kumari, V., van Ijzendoorn, S. C. D., Reyes-Mugica, M., Kumar, A., Gujral, T., Dudeja, P. K. and Ameen, N. A. (2016). Identification of intestinal ion transport defects in microvillus inclusion disease. *Am. J. Physiol. Gastrointest. Liver Physiol.* **311**, G142-G155. doi:10.1152/ajpgi.00041.2016

Lee, S.-K., Li, W., Ryu, S.-E., Rhim, T. Y. and Ahnn, J. (2010). Vacuolar (H+)-ATPases in Caenorhabditis elegans: what can we learn about giant H+ pumps from tiny worms? *Biochim. Biophys. Acta* **1797**, 1687-1695. doi:10.1016/j.bbabio.2010.07.004

Liégeois, S., Benedetto, A., Garnier, J.-M., Schwab, Y. and Labouesse, M. (2006). The V0-ATPase mediates apical secretion of exosomes containing Hedgehog-related proteins in Caenorhabditis elegans. *J. Cell Biol.* **173**, 949-961. doi:10.1083/jcb.200511072

Marion, S., Hoffmann, E., Holzer, D., LE Clainche, C., Martin, M., Sachse, M., Ganeva, I., Mangeat, P. and Griffiths, G. (2011). Ezrin promotes actin assembly at the phagosome membrane and regulates phago-lysosomal fusion. *Traffic* **12**, 421-437. doi:10.1111/j.1600-0854.2011.01158.x

Martin-Belmonte, F., Gassama, A., Datta, A., Yu, W., Rescher, U., Gerke, V. and Mostov, K. (2007). PTEN-mediated apical segregation of phosphoinositides controls epithelial morphogenesis through Cdc42. *Cell* **128**, 383-397. doi:10.1016/j.cell.2006.11.051

Maxson, M. E. and Grinstein, S. (2014). The vacuolar-type H(+)-ATPase at a glance - more than a proton pump. *J. Cell Sci.* **127**, 4987-4993. doi:10.1242/jcs.158550

McGhee, J. D. (2007). The *C. elegans* intestine (ed. The C. elegans Research Community), *WormBook* (http://www.wormbook.org). doi:10.1895/wormbook.1.133.1

Merkulova, M., Păunescu, T. G., Azroyan, A., Marshansky, V., Breton, S. and Brown, D. (2015). Mapping the H(+) (V)-ATPase interactome: identification of proteins involved in trafficking, folding, assembly and phosphorylation. *Sci. Rep.* **5**, 14827. doi:10.1038/srep14827

Michaux, G., Massey-Harroche, D., Nicolle, O., Rabant, M., Brousse, N., Goulet, O., LE Bivic, A. and Ruemmele, F. M. (2016). The localisation of the apical Par/Cdc42 polarity module is specifically affected in microvillus inclusion disease. *Biol. Cell* **108**, 19-28. doi:10.1111/boc.201500034

Morel, N., Dedieu, J. C. and Philippe, J. M. (2003). Specific sorting of the a1 isoform of the V-H+ATPase a subunit to nerve terminals where it associates with both synaptic vesicles and the presynaptic plasma membrane. *J. Cell Sci.* **116**, 4751-4762. doi:10.1242/jcs.00791

Mosa, M. H., Nicolle, O., Maschalidi, S., Sepulveda, F. E., Bidaud-Meynard, A., Menche, C., Michels, B. E., Michaux, G., de Saint Basile, G. and Farin, H. F. (2018). Dynamic formation of microvillus inclusions during enterocyte differentiation in Munc18-2-deficient intestinal organoids. *Cell Mol. Gastroenterol. Hepatol.* **6**, 477-493.e1. doi:10.1016/j.jcmgh.2018.08.001

Müller, T., Hess, M. W., Schiefermeier, N., Pfaller, K., Ebner, H. L., Heinz-Erian, P., Ponstingl, H., Partsch, J., Röllinghoff, B., Köhler, H. et al. (2008). MYO5B mutations cause microvillus inclusion disease and disrupt epithelial cell polarity. *Nat. Genet.* **40**, 1163-1165. doi:10.1038/ng.225

Nicolle, O., Burel, A., Griffiths, G., Michaux, G. and Kolotuev, I. (2015). Adaptation of cryo-sectioning for IEM labeling of asymmetric samples: a study using Caenorhabditis elegans. *Traffic* **16**, 893-905. doi:10.1111/tra.12289

Reinshagen, K., Naim, H. Y. and Zimmer, K. P. (2002). Autophagocytosis of the apical membrane in microvillus inclusion disease. *Gut* **51**, 514-521. doi:10.1136/gut.51.4.514

Rodriguez-Boulan, E. and Macara, I. G. (2014). Organization and execution of the epithelial polarity programme. *Nat. Rev. Mol. Cell Biol.* **15**, 225-242. doi:10.1038/nrm3775

Ruemmele, F. M., Schmitz, J. and Goulet, O. (2006). Microvillous inclusion disease (microvillous atrophy). *Orphanet J. Rare Dis.* **1**, 22. doi:10.1186/1750-1172-1-22

Saegusa, K., Sato, M., Sato, K., Nakajima-Shimada, J., Harada, A. and Sato, K. (2014). Caenorhabditis elegans chaperonin CCT/TRiC is required for actin and tubulin biogenesis and microvillus formation in intestinal epithelial cells. *Mol. Biol. Cell* **25**, 3095-3104. doi:10.1091/mbc.e13-09-0530

Sato, M., Saegusa, K., Sato, K., Hara, T., Harada, A. and Sato, K. (2011). Caenorhabditis elegans SNAP-29 is required for organellar integrity of the endomembrane system and general exocytosis in intestinal epithelial cells. *Mol. Biol. Cell* **22**, 2579-2587. doi:10.1091/mbc.e11-04-0279

Schneeberger, K., Vogel, G. F., Teunissen, H., van Ommen, D. D., Begthel, H., EL Bouazzaoui, L., van Vugt, A. H. M., Beekman, J. M., Klumperman, J., Müller, T. et al. (2015). An inducible mouse model for microvillus inclusion disease reveals a role for myosin Vb in apical and basolateral trafficking. *Proc. Natl. Acad. Sci. USA* **112**, 12408-12413. doi:10.1073/pnas.1516672112

Schneeberger, K., Roth, S., Nieuwenhuis, E. E. S. and Middendorp, S. (2018). Intestinal epithelial cell polarity defects in disease: lessons from microvillus inclusion disease. *Dis. Model. Mech.* **11**, dmm031088. doi:10.1242/dmm.031088

Shafaq-Zadah, M., Brocard, L., Solari, F. and Michaux, G. (2012). AP-1 is required for the maintenance of apico-basal polarity in the C. elegans intestine. *Development* **139**, 2061-2070. doi:10.1242/dev.076711

Sidhaye, J., Pinto, C. S., Dharap, S., Jacob, T., Bhargava, S. and Sonawane, M. (2016). The zebrafish goosepimples/myosin Vb mutant exhibits cellular attributes of human microvillus inclusion disease. *Mech. Dev.* **142**, 62-74. doi:10.1016/j.mod.2016.08.001

Sobajima, T., Yoshimura, S.-I., Iwano, T., Kunii, M., Watanabe, M., Atik, N., Mushiake, S., Morii, E., Koyama, Y., Miyoshi, E. et al. (2015). Rab11a is required for apical protein localisation in the intestine. *Biol Open* **4**, 86-94. doi:10.1242/bio.20148532

Sobota, J. A., Back, N., Eipper, B. A. and Mains, R. E. (2009). Inhibitors of the V0 subunit of the vacuolar H+-ATPase prevent segregation of lysosomal- and secretory-pathway proteins. *J. Cell Sci.* **122**, 3542-3553. doi:10.1242/jcs.034298

Steegmaier, M., Yang, B., Yoo, J. S., Huang, B., Shen, M., Yu, S., Luo, Y. and Scheller, R. H. (1998). Three novel proteins of the syntaxin/SNAP-25 family. *J. Biol. Chem.* **273**, 34171-34179. doi:10.1074/jbc.273.51.34171

Sudhof, T. C. and Rothman, J. E. (2009). Membrane fusion: grappling with SNARE and SM proteins. *Science* **323**, 474-477. doi:10.1126/science.1161748

Talmon, G., Holzapfel, M., Dimaio, D. J. and Muirhead, D. (2012). Rab11 is a useful tool for the diagnosis of microvillous inclusion disease. *Int. J. Surg. Pathol.* **20**, 252-256. doi:10.1177/1066896911430959

Vacca, B., Bazellières, E., Nouar, R., Harada, A., Massey-Harroche, D. and LE Bivic, A. (2014). Drebrin E depletion in human intestinal epithelial cells mimics Rab8a loss of function. *Hum. Mol. Genet.* **23**, 2834-2846. doi:10.1093/hmg/ddt670

Vogel, G. F., Klee, K. M. C., Janecke, A. R., Müller, T., Hess, M. W. and Huber, L. A. (2015). Cargo-selective apical exocytosis in epithelial cells is conducted by Myo5b, Slp4a, Vamp7, and Syntaxin 3. *J. Cell Biol.* **211**, 587-604. doi:10.1083/jcb.201506112

Vogel, G. F., Hess, M. W., Pfaller, K., Huber, L. A., Janecke, A. R. and Müller, T. (2016). Towards understanding microvillus inclusion disease. *Mol. Cell. Pediatr.* **3**, 3. doi:10.1186/s40348-016-0031-0

Vogel, G. F., Janecke, A. R., Krainer, I. M., Gutleben, K., Witting, B., Mitton, S. G., Mansour, S., Ballauff, A., Roland, J. T., Engevik, A. C. et al. (2017a). Abnormal Rab11-Rab8-vesicles cluster in enterocytes of patients with microvillus inclusion disease. *Traffic* **18**, 453-464. doi:10.1111/tra.12486

Vogel, G. F., van Rijn, J. M., Krainer, I. M., Janecke, A. R., Posovszky, C., Cohen, M., Searle, C., Jantchou, P., Escher, J. C., Patey, N. et al. (2017b). Disrupted apical exocytosis of cargo vesicles causes enteropathy in FHL5 patients with Munc18-2 mutations. *JCI Insight* **2**, e94564. doi:10.1172/jci.insight.94564

Weis, V. G., Knowles, B. C., Choi, E., Goldstein, A. E., Williams, J. A., Manning, E. H., Roland, J. T., Lapierre, L. A. and Goldenring, J. R. (2016). Loss of MYO5B in mice recapitulates Microvillus Inclusion Disease and reveals an apical trafficking pathway distinct to neonatal duodenum. *Cell Mol. Gastroenterol. Hepatol.* **2**, 131-157. doi:10.1016/j.jcmgh.2015.11.009

Wiegerinck, C. L., Janecke, A. R., Schneeberger, K., Vogel, G. F., van Haaften-Visser, D. Y., Escher, J. C., Adam, R., Thoni, C. E., Pfaller, K., Jordan, A. J. et al. (2014). Loss of syntaxin 3 causes variant microvillus inclusion disease. *Gastroenterology* **147**, 65-68.e10. doi:10.1053/j.gastro.2014.04.002

Winter, J. F., Höpfner, S., Korn, K., Farnung, B. O., Bradshaw, C. R., Marsico, G., Volkmer, M., Habermann, B. and Zerial, M. (2012). Caenorhabditis elegans screen reveals role of PAR-5 in RAB-11-recycling endosome positioning and apicobasal cell polarity. *Nat. Cell Biol.* **14**, 666-676. doi:10.1038/ncb2508

Zhang, H., Abraham, N., Khan, L. A., Hall, D. H., Fleming, J. T. and Göbel, V. (2011). Apicobasal domain identities of expanding tubular membranes depend on glycosphingolipid biosynthesis. *Nat. Cell Biol.* **13**, 1189-1201. doi:10.1038/ncb2328

Zhang, H., Kim, A., Abraham, N., Khan, L. A., Hall, D. H., Fleming, J. T. and Gobel, V. (2012). Clathrin and AP-1 regulate apical polarity and lumen formation during C. elegans tubulogenesis. *Development* **139**, 2071-2083. doi:10.1242/dev.077347

Zhu, H., Sewell, A. K. and Han, M. (2015). Intestinal apical polarity mediates regulation of TORC1 by glucosylceramide in C. elegans. *Genes Dev.* **29**, 1218-1223. doi:10.1101/gad.263483.115